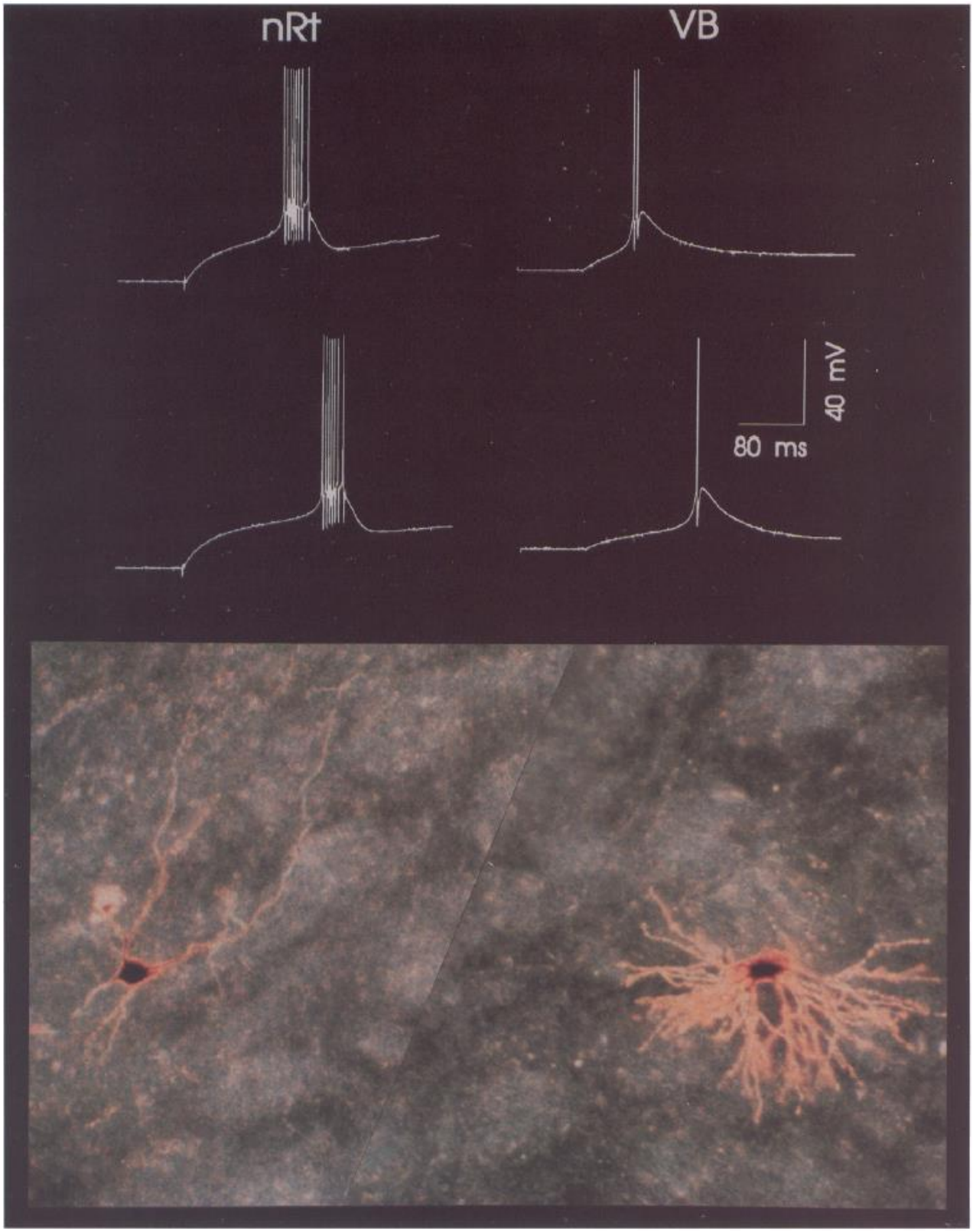

Huguenard & Prince 1992

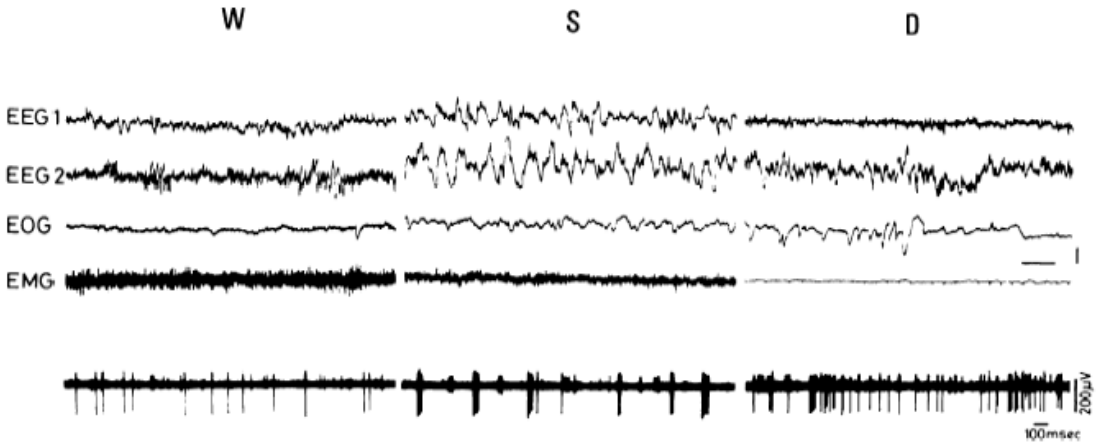

FIG. 2. Electrographic data (top) and cathode-ray oscilloscope (CRO) display of recordings of typical unit activity during waking, slow wave, and desynchronized sleep. Note the characteristic burst pattern that developed in S, replacing the single-spike discharge in W. D showed a few bursts and an overall increase in discharge frequency. Electrographic data: time calibration = 1 s, voltage = 200 μV for EEG 1 (suprasylvian) and EEG 2 (marginal gyrus) and 500 μV for EOG and EMG.

McCarley et al. 1983

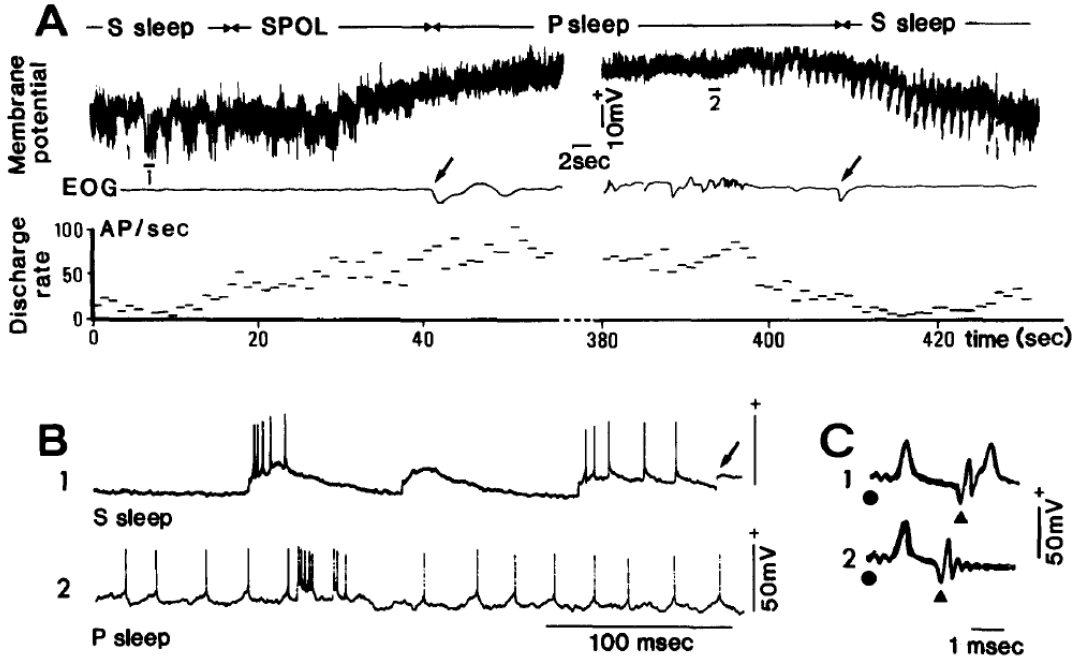

Fig. 1. Tonic depolarization of an LGB realy neuron during P sleep. A: simultaneous display of behavioral state. DC cell recording (filtered at 0–75 Hz), eye movements (EOG) and discharge rate of action potentials (bin width: 1 s). Left-hand side: neuron depolarized during SPOL and had already depolarized by 8 mV when the animal entered P sleep (t = 41 s, first eye movement, arrow). Depolarization was maintained throughout P sleep; only the beginning and the end of the episode is presented (320 s elapsed between left and right sets of traces). Right-hand side: upon last eye movement (arrow) of P sleep the neuron repolarized as the animal went back to S sleep. B: enlarged segments (labelled 1 and 2 under cell trace in A) of spontaneous activity. B_1: S sleep activity was composed of isolated EPSPs (arrow) that did not always fire the cell and of large depolarizations with or without a burst of spikes. B_2: during P sleep action potentials arose from small depolarizations. The rapid discharge was disrupted by short depolarizations which gave birth to a cluster of spikes of decreasing amplitude. C: identification of neuron. C_1: orthodromic response to optic tract stimulation (circle), antidromic action potentials to visual radiation stimulation (triangle). C_2: positive collision test. Five traces superimposed.

Hirsch et al. 1983

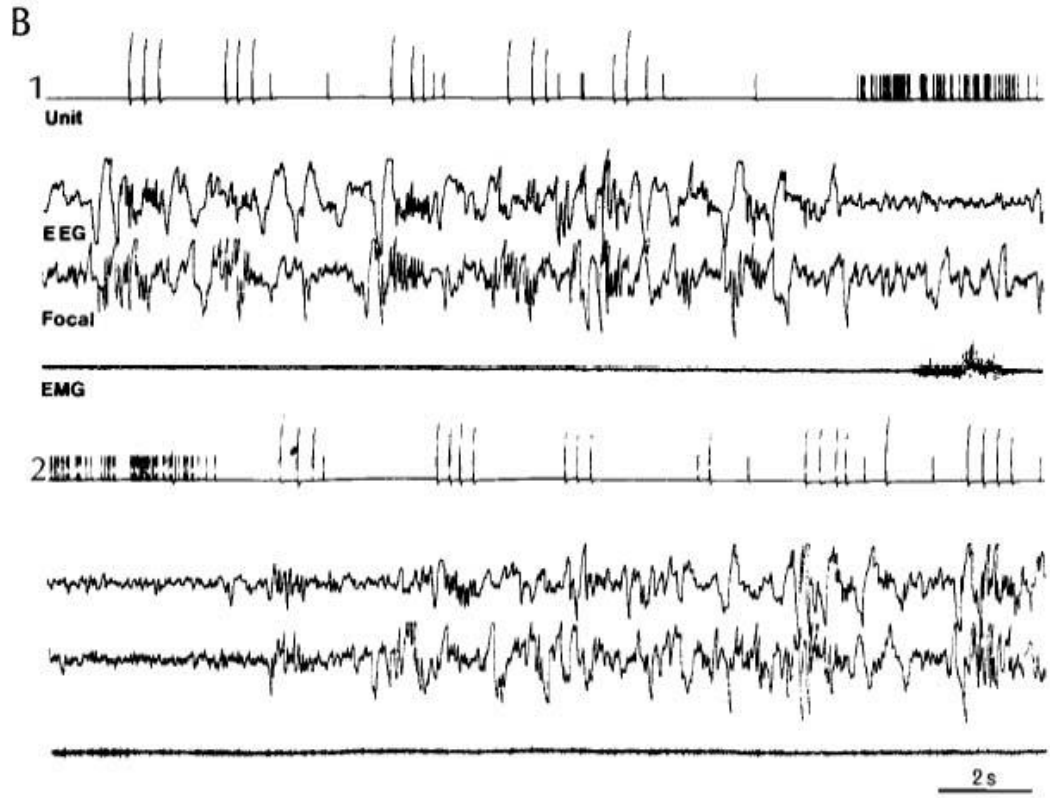

Figure 4. Discharge patterns during transitions from S to W and W to S. Two neurons projecting to the parietal (*A*) and motor (*B*) cortices are shown, *neuron B* is the same as depicted in Figure 3*B*. Unit spikes displayed on the oscilloscope were used to trigger an ink pen galvanometer. The larger deflections represent a burst of high frequency spikes. Note the strikingly different discharge patterns which correlate to EEG activity and other electrographic signs of the behavioral state. Also note (in B_1 and $_2$) the correlation between sequences of spike bursts and grouped spindle waves as recorded from the cortical surface (*EEG*) and the thalamic microelectrode (*focal*). *EOG*, Electro-oculogram.

Glenn & Steriade 1982

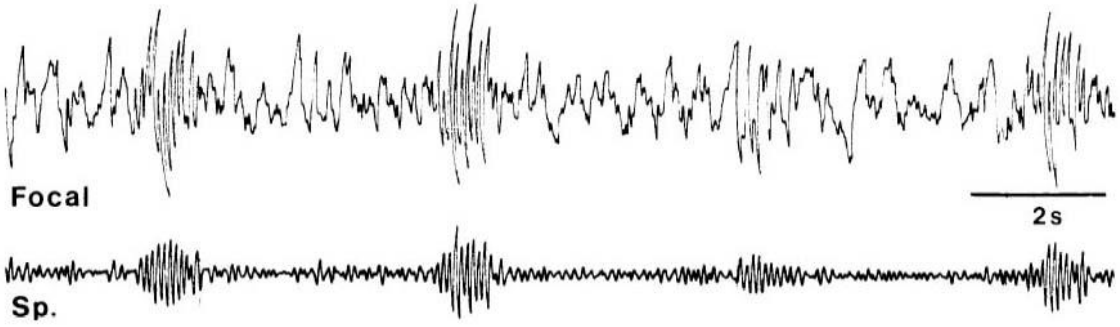

FIG. 6.

Unanesthetized cerveau isolé preparation.
extracellular recordings of a central lateral (CL)
Focal thalamic waves, simultaneously recorded by the same microelectrodes
as recorded (Focal), after passage through a 7- to 14-Hz band-pass filter to depict spindles

Pare et al.1987

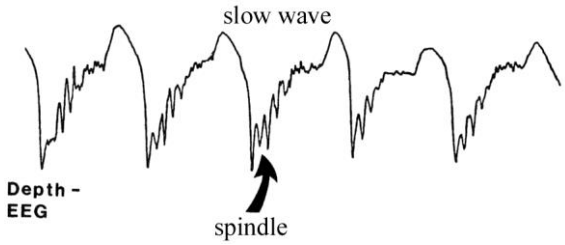

slow waves: 0.5-4 Hz
spindles: 7-14 Hz

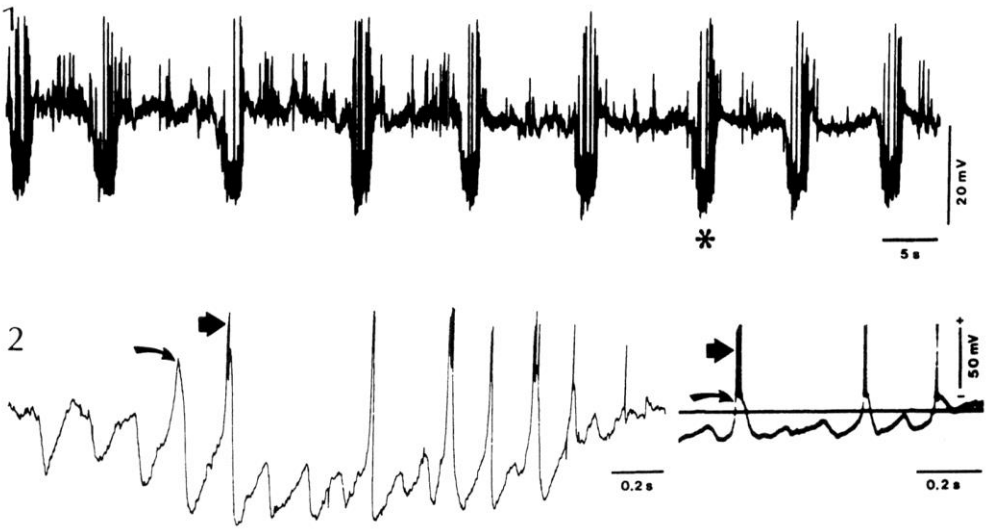

FIG. 4. Spontaneous rhythmic episodes of membrane potential oscillations in a thalamic relay neuron located in the VL nucleus. Spindle sequence marked by an asterisk is depicted below at a faster speed. Traces 1 and 2 are polygraphic recordings. Oscilloscopic recording appears in the right-hand trace in 2. Curved and straight arrows indicate, respectively, the low-threshold Ca spike and somatic burst discharges. In the interspindle lull the membrane potential was −63 mV.

Deschenes et al. 1984

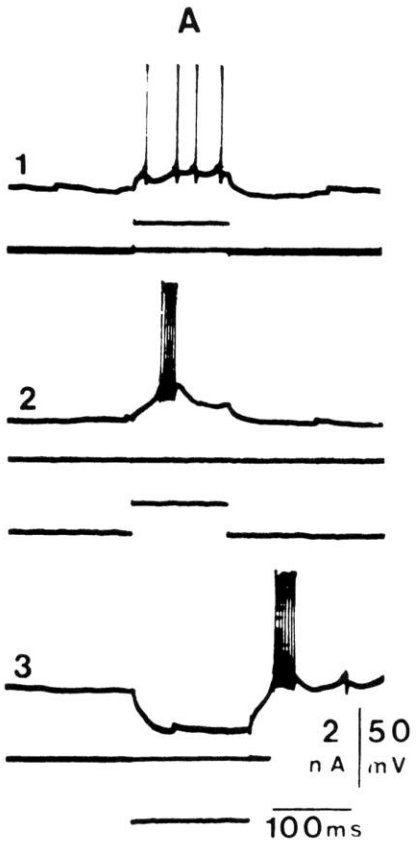

FIG. 12. Effect of membrane potential on the firing mode of thalamic relay neurons. In A_1 where resting membrane potential was at −62 mV, an 0.8-nA depolarizing current pulse triggered tonic firing in this VPL relay neuron, while during hyperpolarization of the cell membrane to −70 mV, the same depolarizing pulse triggered burst discharges on the crest of a low-threshold Ca spike (A_2). Postanodal burst discharges could also be triggered at the break of a hyperpolarizing pulse (A_3).

Deschenes et al. 1984

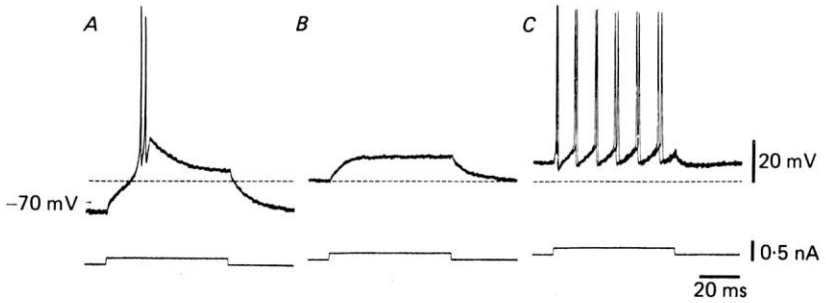

Fig. 2. Stimulation of thalamic cell with a constant amplitude transmembrane current pulse at three different membrane potentials. In this and the following Figures the resting potential of the cell is given in mV and its level indicated to the left with an arrow. In *A* the cell was directly stimulated while being hyperpolarized by a constant current injection. The outward current pulse triggers an all-or-none burst of spikes. In *B* the same current pulse produces a subthreshold depolarization if superimposed on a slightly depolarized membrane potential level. In *C*, after further depolarization by a direct current, the current pulse produce a train of action potentials. Dashed line serves as a reference level which indicates a low excitability point between *A* and *C*. Note the different firing levels in records *A* and *C*.

Jahnsen & Llinas 1984

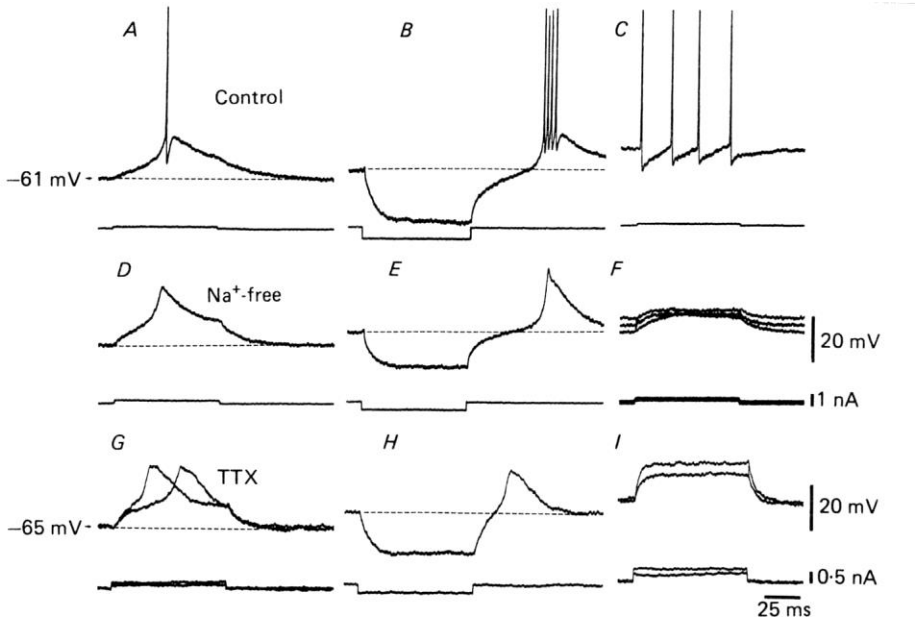

Fig. 2. Dependence of fast spikes on Na^+. *A*, *B* and *C*, control. Depolarizing current pulse from rest elicited a small burst response (*A*). Hyperpolarizing current pulse after d.c. depolarization of cell produced a rebound response (*B*), and a depolarizing pulse from a depolarized level elicited a train of fast spikes (*C*). *D*, *E* and *F*, after replacement of NaCl by choline Cl, the fast component of the burst response (*D* and *E*), and the fast action potentials (*F*) disappeared. The slow component of the burst was unchanged. *G*, *H* and *I*, in a different cell, tetrodotoxin (TTX) had the same effect as removal of NaCl.

Jahnsen & Llinas 1984

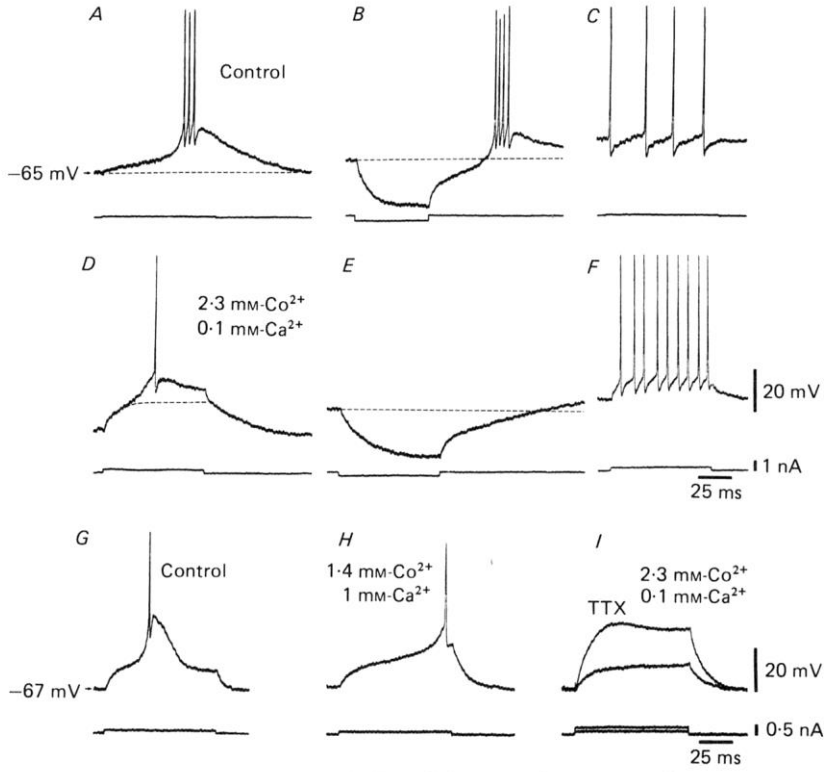

Fig. 4. Effect of blocking g_{Ca} on l.t.s. *A*, *B* and *C*, control responses. Burst response (*A*), rebound burst response (*B*), and fast spikes (*C*). *D*, *E* and *F*, 5 min after addition of Co^{2+} and reduction of Ca^{2+}, the burst response (at rest) (*D*) and the rebound response (*E*) are blocked but fast spikes are not affected (*D* and *F*). *G*, *H* and *I*, complete block of burst response in another cell after reduction of the Ca^{2+} concentration and addition of Co^{2+} to the solution. *G*, control response. *H*, after 15 min only the fast spike and a slowly rising potential remained. *I*, addition of TTX completely blocked the active responses.

Jahnsen & Llinas 1984

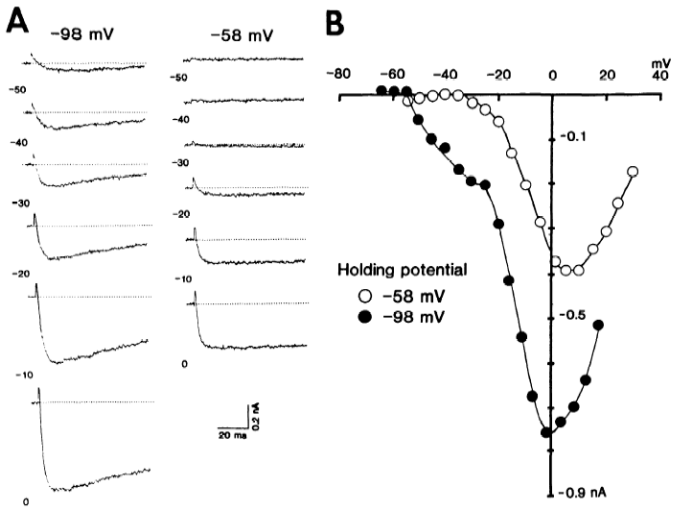

FIG. 4. Whole-cell Ca currents in acutely dissociated LGN neurons. Separation of 2 components based on holding potential. External medium contained 5 mM Ca^{2+} and no Na^{+}. Pipette *solution B*; containing 10 mM Cs-EGTA (see METHODS). *A*: membrane potential was held at either −98 mV (*left*) or −58 mV (*right*) and then stepped to a series of 75-ms test potentials as indicated near each trace. Note transient currents at low membrane potentials (−30, −40 mV) and slowly decaying currents at stronger depolarizations. *B*: current-to-voltage relationship of the peak Ca currents from *A*, obtained from holding potentials (HP) at −98 mV (filled circles) and −58 mV (open circles). Note that a component activated at low voltages is present when test pulses are applied from HP = −98 mV and absent at HP = −58 mV. The second component, activated at higher voltages, is considerably less reduced with depolarization.

Hernandez-Cruz & Pape1989

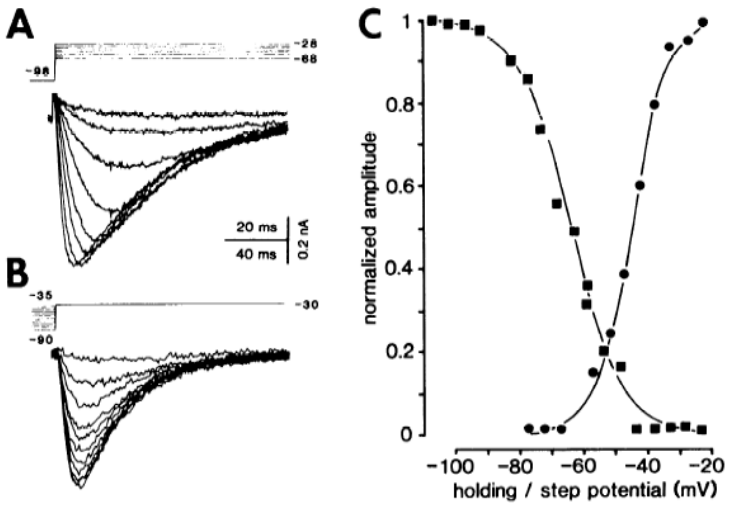

FIG. 6. Activation and inactivation of the transient, low-voltage-activated (LVA) Ca current. *A*: current records in response to 75-ms depolarizing steps starting at −68 and ending at −28 mV in 5-mV increments from HP = −98 mV. *B*: records obtained in the same cell following a 200-ms test step to −30 mV when the HP (300-ms prepulse) was varied from −90 to −35 in 5-mV increments. *C*: normalized peak current amplitudes plotted against membrane potential (filled circles; data from *A* included) and holding potential (filled squares; data from *B* included). Data points represented by filled squares were fitted with the Boltzmann relation $I/I_{max} = \{1 + \exp[(V - V_{1/2})/k]\}^{-1}$, where I is peak current, I_{max} is the maximal current from an HP of −110 mV, V is the holding potential, $V_{1/2}$ is the half-inactivation value, and k is the steepness parameter. The data points represented by filled circles were fitted with the expression $I/I_{max} = \{1 + \exp[-(V - V_{1/2})/k]\}^{-1}$, where I_{max} is the peak current at −23 mV, and V is the test pulse membrane potential. Pipette contained 10 mM Cs-BAPTA. Postnatal day 16.

Hernandez-Cruz & Pape1989

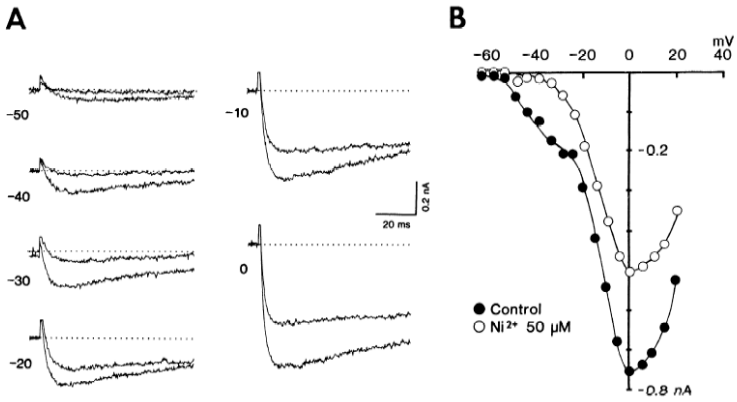

FIG. 8. Preferential block of transient Ca currents by Ni^{2+}. *A*: from an HP of −98 mV, 75-ms step potentials to the indicated voltages were applied in control medium and after 3-min superfusion with 50 µM Ni^{2+}. Control and test traces are superimposed. Records in Ni^{2+} are the ones with smaller amplitude for each membrane potential. Blocking effects are considerably greater on the transient than on the sustained currents. *B*: peak current-to-voltage relationship obtained from the complete set of records exemplified in *A*. Currents in control medium and in 50 µM Ni^{2+} are plotted as filled and open circles, respectively. Note similarity with effects of changing the HP to more depolarized levels (Fig. 4*B*). In both cases, the current component activated at low membrane potentials is selectively suppressed. Data in Figs. 4 and 8 have been obtained from the same cell. Pipette contained 10 mM Cs-EGTA.

Hernandez-Cruz & Pape1989

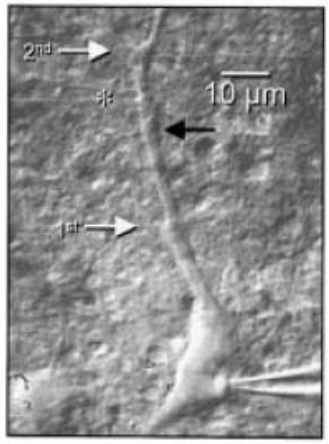

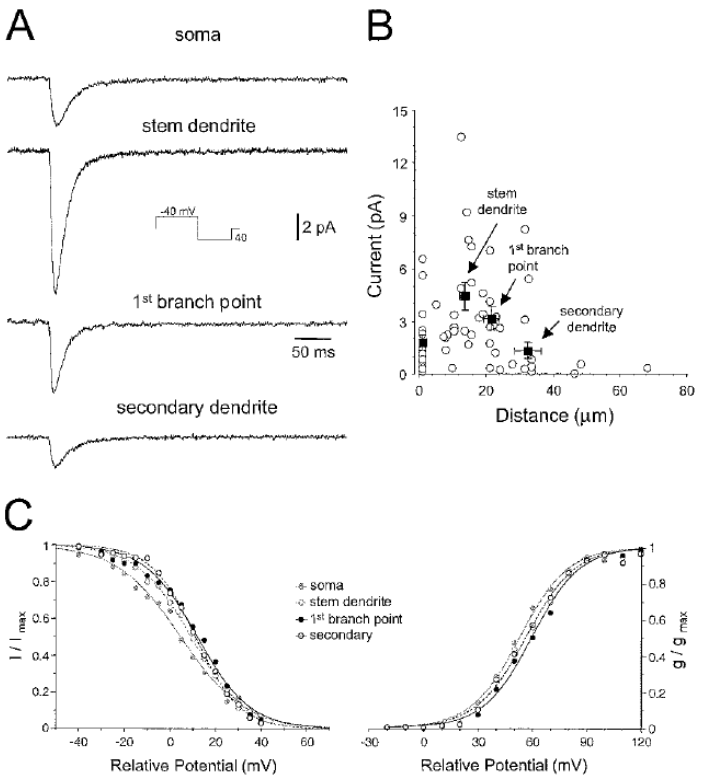

Figure 9. Somato-dendritic distribution and properties of low-threshold calcium channels. *A*, Selected averaged traces demonstrating the relationship between current amplitude and recording location. Note that the transient inward current is of the same kinetics at each recording location, but of relatively greater amplitude when recorded from stem dendrites. Somatic and stem dendritic patches were taken from the same neuron. *B*, Pooled data quantifying the relationship between current density and dendritic location. Each recording is shown as an *open circle*. *Filled squares* show mean (±SD) current as a function of distance from the soma (±SD) for recordings made from the soma, stem dendrites, primary branch points, and higher order dendrites (from *left* to *right*, respectively). *C*, Steady-state activation and inactivation curves constructed from data pooled by recording location, as shown in the *inset*. Note that more distal dendritic recordings yield activation and inactivation curves that are shifted to the right along the voltage axis. Voltages are relative to resting membrane potential.

Williams & Stuart 2000

Channel name	$Ca_v3.1$
Description	voltage-gated calcium channel α_1 subunit
Other names	T-type, α_{1G}, $Ca_vT.1$
Molecular information	human: 2171aa, O43497, NP_061496, chr. 17q22, *CACNA1G* (ref. 1) rat: 2254aa, O54898, AAC67372, mouse: 2288aa, Q9WUB8, NP_033913 (see Comments)
Associated subunits	no biochemical evidence, small changes induced by $\alpha_2\delta_1$ (ref. 2) and $\alpha_2\delta_2$ (refs. 3,4)
Functional assays	voltage clamp, calcium imaging
Current	$I_{Ca,T}$
Conductance	7.5pS (ref. 1)
Ion selectivity	$Sr^{2+} > Ba^{2+} = Ca^{2+}$ (ref. 5)
Activation	$V_a = -46mV$; τ_a = 1ms at −10mV (ref. 6)
Inactivation	$V_h = -73mV$; τ_h = 11ms at −10mV (ref. 6)
Activators	not established
Gating inhibitors	kurtoxin, IC_{50} = 15nM (ref. 7)
Blockers	no sub-type specific blocker[8] selective for $Ca_v3.x$ relative to $Ca_v1.x$ and $Ca_v2.x$: mibefradil[9,10], U92032 (ref. 11), and pimozide[12] non-selective: nickel (IC_{50} = 250μM)[13], amiloride[14]
Radioligands	none
Channel distribution	brain, especially soma and dendrites of neurones in olfactory bulb, amygdala, cerebral cortex, hippocampus, thalamus, hypothalamus, cerebellum, brain stem (human RNA blots[1,5], rat *in situ* hybridisation[15,18] and immunocytochemistry[16]); ovary[5], placenta[5], heart (especially sinoatrial node; mouse *in situ* hybridisation)
Physiological functions	thalamic oscillations[18,19], possibly cardiac pacemaking
Mutations and pathophysiology	not established
Pharmacological significance	thalamocortical dysrhythmias[19,20]
Comments	Splice variants that differ in their voltage dependence have been cloned[5].

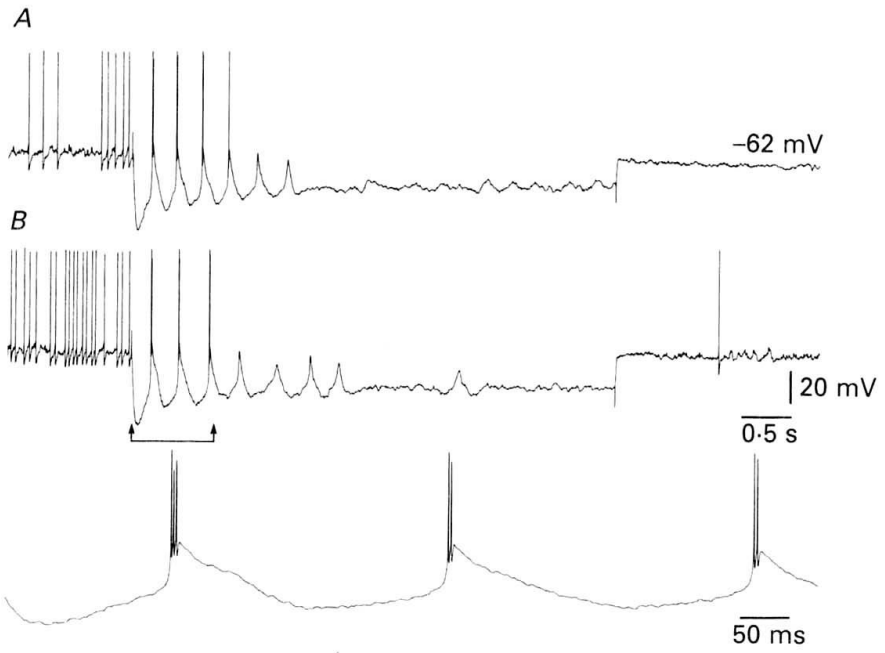

Fig. 2. Induced delta oscillation in a neurone with intact cortical afferents. *A* and *B* represent the same VL thalamocortical cells, switched from tonic to slow oscillatory mode by injecting 2 nA hyperpolarizing current pulses. Note the dampening of the oscillation with appearance of subthreshold events as the slow V_m relaxation progressively depolarized the membrane. Upon removal of the pulse, V_m recovered after a tail depolarization. The portion between arrows in *B* is depicted in the bottom part at higher speed, to show high-frequency bursts of spikes crowning the LTSs, each of them triggered by a pacemaker depolarization.

Curro et al. 1992

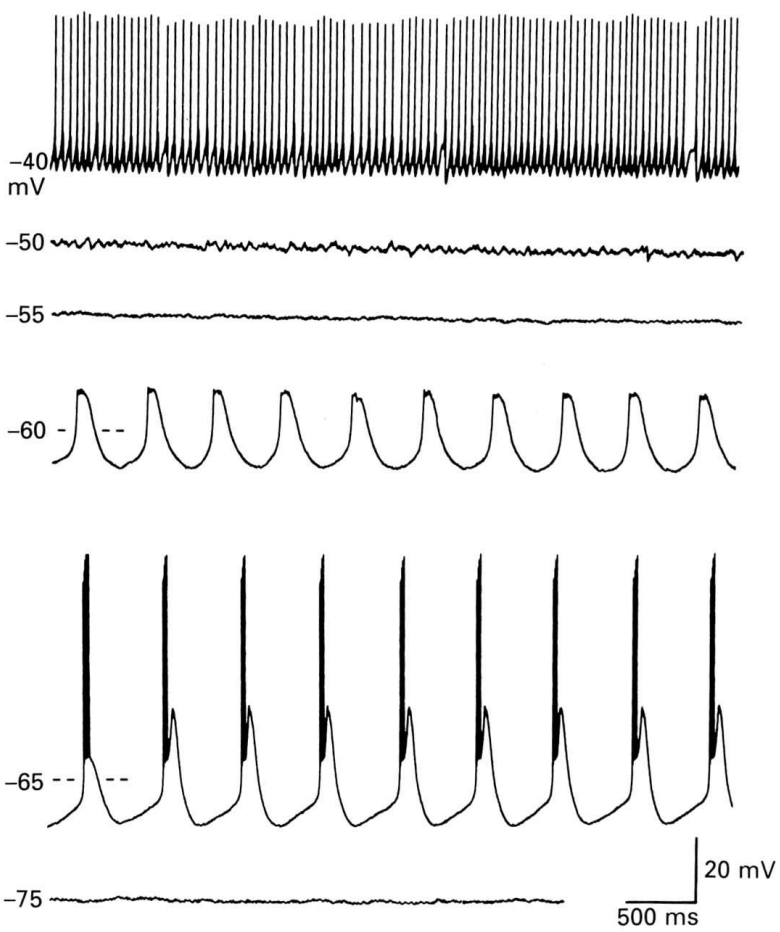

Fig. 2. Voltage dependence of the pacemaker oscillations. Intracellular voltage recordings from a TC cell in the cat dLGN show that the pacemaker oscillations were observed only when the membrane potential was moved (by steady DC current injection) to between −57 and −73 mV. Note that in the trace marked −60 mV the large depolarizations have a higher frequency and a smaller amplitude than those in the trace marked −65 mV. In addition, ramp-like (i.e. pacemaker) depolarizations were evident in the trace marked −65 mV but their absence at more depolarized potentials (traced marked −60 mV) gave the hyperpolarizing phase of the oscillations a more rounded shape. At potentials negative to −73 mV no activity was observed, while at potentials positive to −45 mV the activity of the cell was characterized by continuous firing consisting of single action potentials that showed no accommodation.

Leresche et al. 1991

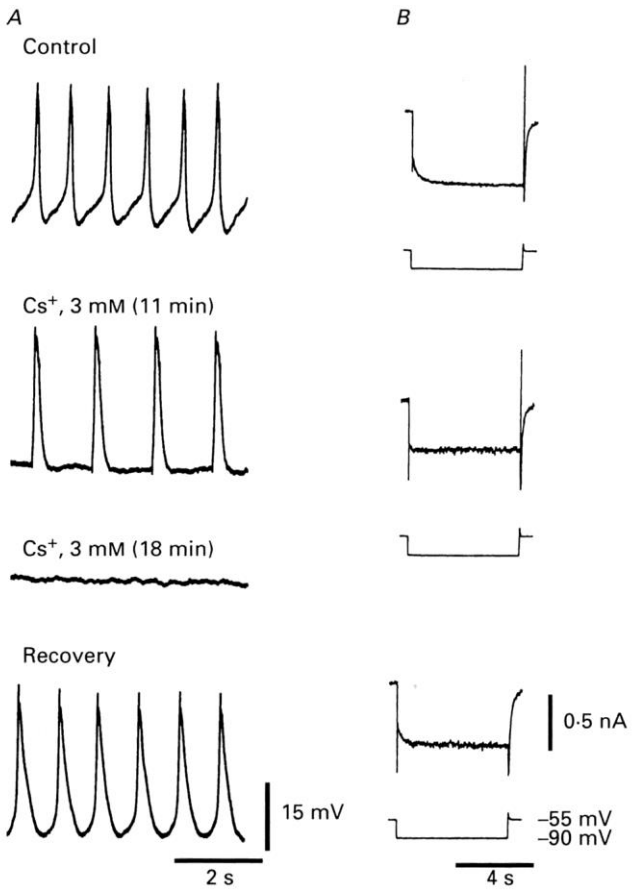

Fig. 4. The effects of Cs^+ on the pacemaker oscillations and on I_h. *A*, intracellular voltage traces show the reversible blockade by 3 mM-Cs^+ of the pacemaker oscillations in a TC cell of the cat dorsal lateral geniculate nucleus (dLGN; membrane potential at the peak of the hyperpolarization, −75 mV). Action potential height has been reduced by the frequency response of the chart recorder. The voltage clamp records in *B* show the concomitant reversible blockade of I_h by Cs^+ in the same cell and were taken immediately after the traces shown in *A*. The transient inward current evoked at the end of the hyperpolarizing voltage step is I_T which was not ideally clamped because of the unfavourable Ca^{2+}/Mg^{2+} concentration ratio (cf. Crunelli *et al.* 1989).

Soltesz et al. 1991

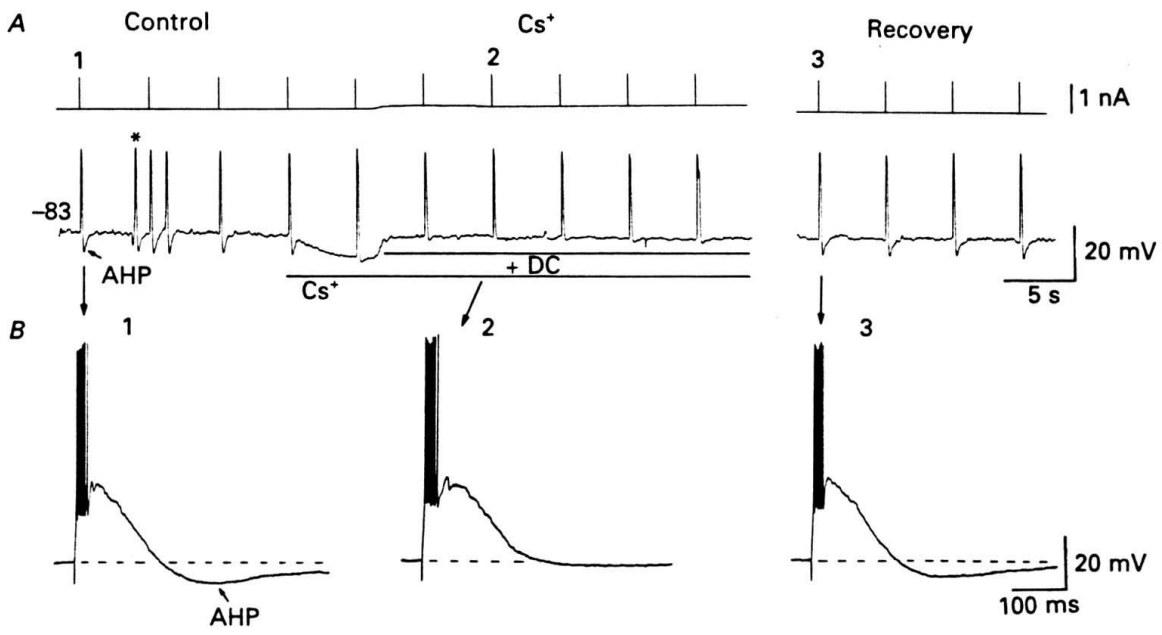

Fig. 12. Local application of Cs^+ blocks the burst after-hyperpolarization (AHP). *A*, intracellular injection of a short duration (3 ms) depolarizing current pulse into a cat LGND neurone at −83 mV results in a burst of six action potentials, followed by an AHP (*A*1 and *B*1), which can occasionally trigger rhythmic activity (asterisk). Local application of Cs^+ (10 mM) results in a hyperpolarization of the membrane potential and a reduction in the amplitude of the AHP. Compensation for the hyperpolarization with intracellular injection of current (+DC) reveals that the AHP is greatly reduced or abolished (*A*2 and *B*2). This effect is reversible (*A*3 and *B*3).

McCormick&Pape1990

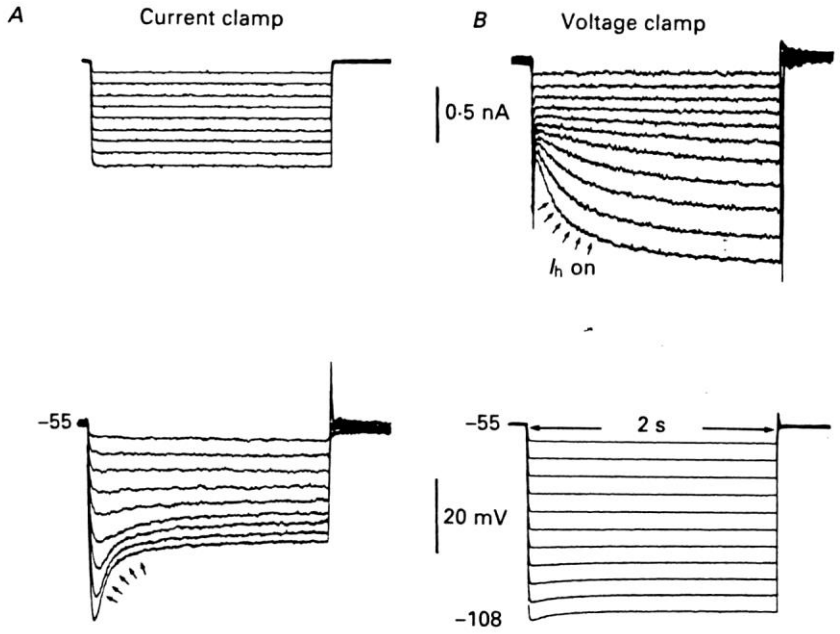

Fig. 1. Rectification of hyperpolarizing responses evoked in a guinea-pig LGND relay cell. Upper traces are membrane current; lower traces are membrane potential. Recordings are from the same cell, depolarized to −55 mV. *A*, in current clamp conditions hyperpolarizing current pulses (duration 1·9 s) evoke membrane hyperpolarizations that show a voltage- and time-dependent depolarizing 'sag' (arrows). *B*, under voltage clamp conditions, hyperpolarizing voltage steps elicit a slow inward current (I_h, arrows) whose amplitude and rate of activation increase with increasing hyperpolarization.

McCormick&Pape1990

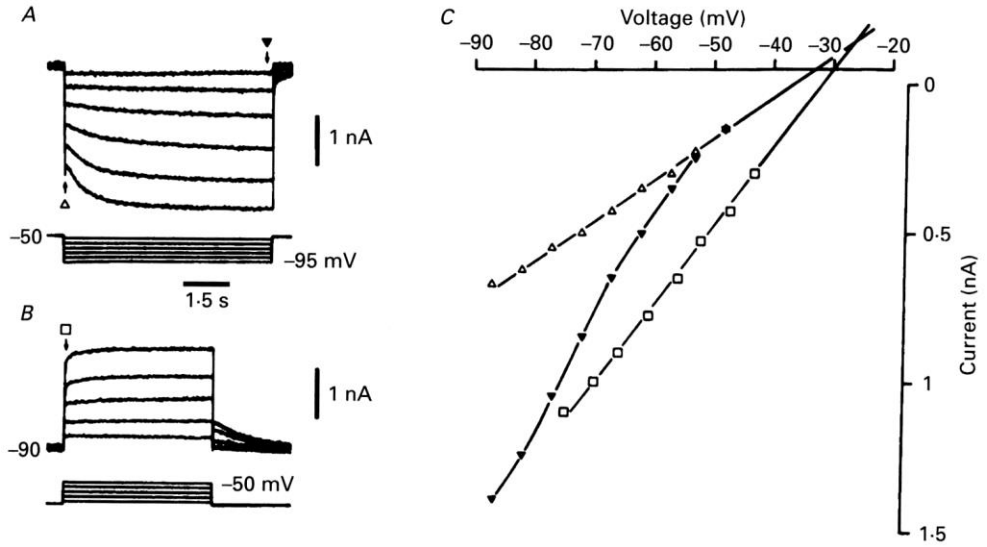

Fig. 2. The reversal potential and activation curve of I_h. *A* shows the development of I_h at different membrane potentials following hyperpolarizing steps from a holding potential of −50 mV. *B* shows tail currents due to the inactivation of I_h following depolarizing steps from a holding potential of −90 mV. In *C*, the instantaneous currents following the hyperpolarizing steps from −50 mV (△) and the depolarizing steps from −90 mV (□) have been measured in another cell and plotted against voltage. These two instantaneous current–voltage plots were linear and, when extrapolated, their intersection gave a reversal potential for I_h of −27·4 mV. The steady-state current, measured 7 s after stepping to each level in *A* (▼), forms an inwardly rectifying relationship with voltage as clearly shown in *C* (▼).

Soltesz et al. 1991

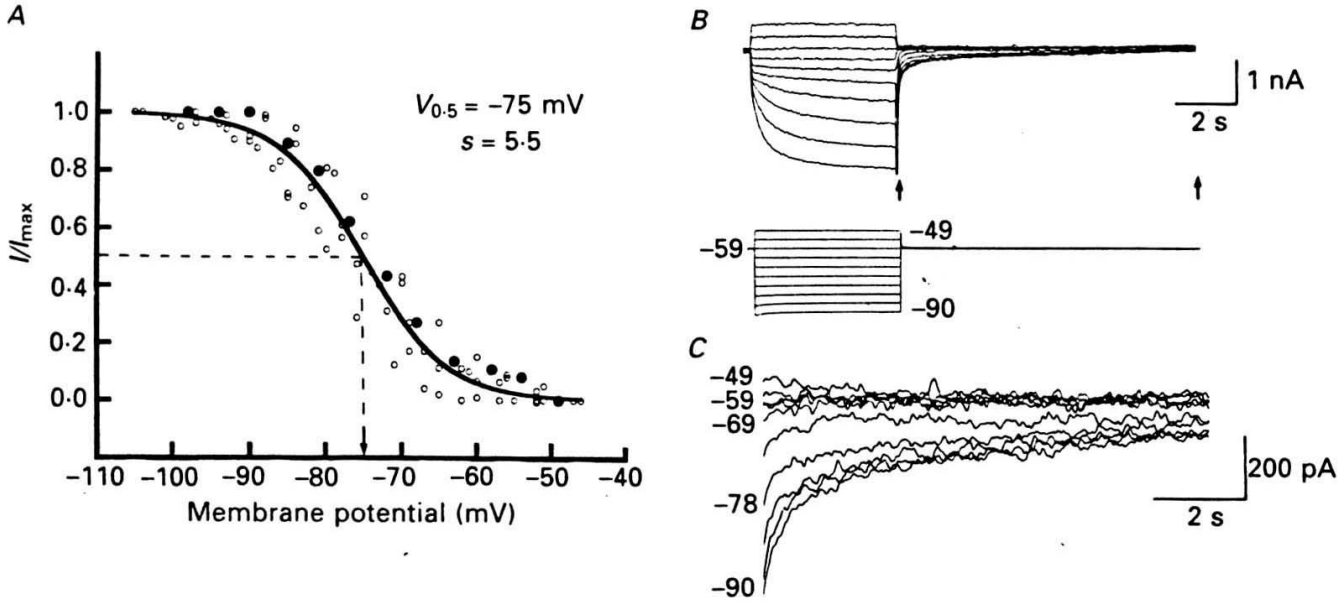

Fig. 2. Activation curve of the conductance, G_h, which underlies I_h. *A*, plot of the activation curve for G_h for seven different LGND relay neurones. Filled circles represent data obtained from cell illustrated in *B* and *C*. Line represents best fit using eqn (1) for data illustrated. *B*, incremental increases in hyperpolarizing steps from −40 to −90 mV progressively increase the amount of I_h which is activated. Tail currents between arrows are expanded for detail in *C*. Care was taken in measuring tail currents so as to minimize the contribution of capacitative or non-I_h active currents by allowing sufficient time for these events to dissipate before measuring I_h. See text for details.

McCormick&Pape1990

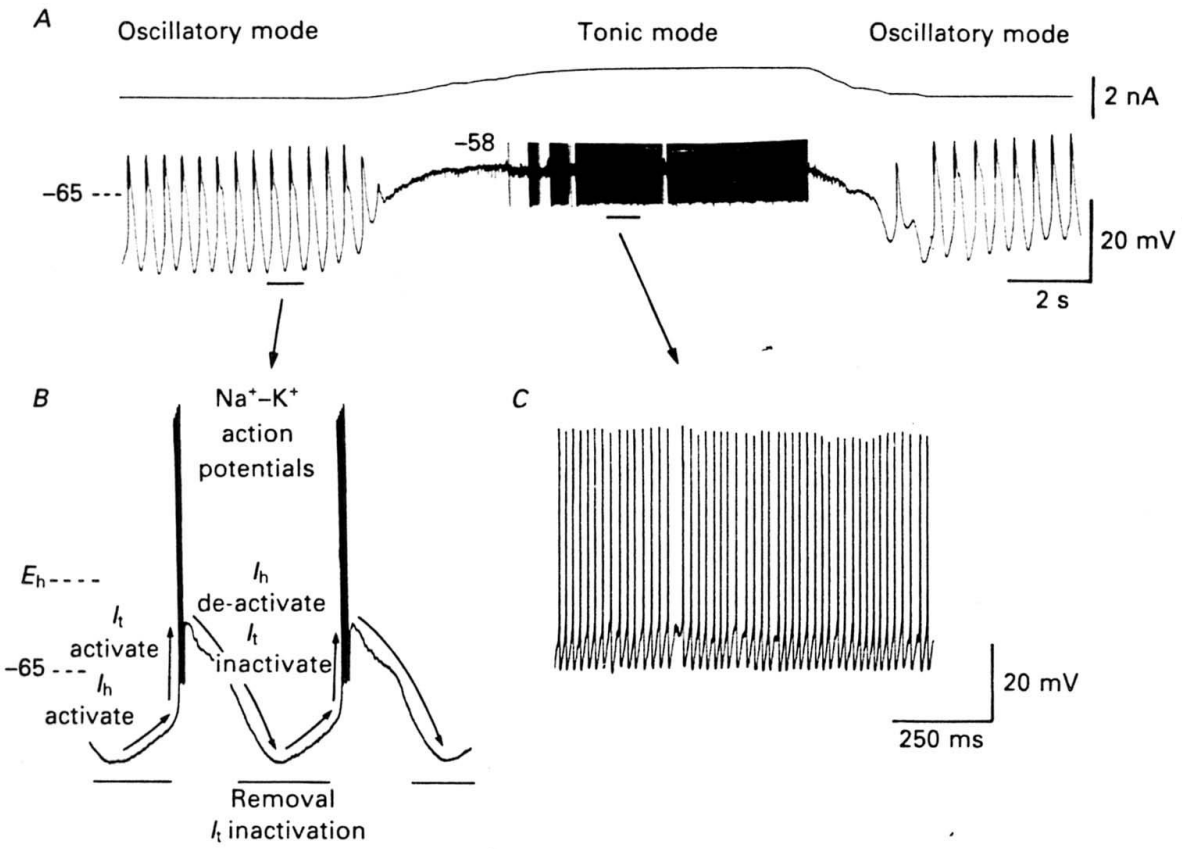

Fig. 14. Two different firing modes of thalamic relay neurones and the proposed ionic substrate of rhythmic burst firing. *A*, this cat LGND neurone generated rhythmic burst firing at a rate of about 2 Hz. Depolarization of the cell to −58 mV with the intracellular injection of current (top trace) halted the rhythmic activity and switched the neurone to the tonic, or single-spike, mode of action potential generation. Removal of the depolarization reinstated the oscillatory activity. *B*, expanded trace of oscillatory activity and the proposed currents which largely mediate it. Activation of the low-threshold calcium current, I_t, depolarizes the membrane towards threshold for a burst of Na^+- and K^+-dependent fast action potentials. The depolarization de-activates the portion of I_h that was active immediately before the Ca^{2+} spike. Repolarization of the membrane due to I_t inactivation is followed by a hyperpolarizing overshoot, due to the reduced depolarizing effect of I_h. The hyperpolarization in turn de-inactivates I_t and activates I_h, which depolarizes the membrane towards threshold for another Ca^{2+} spike. *C*, expanded trace of single-spike activity.

McCormick&Pape1990

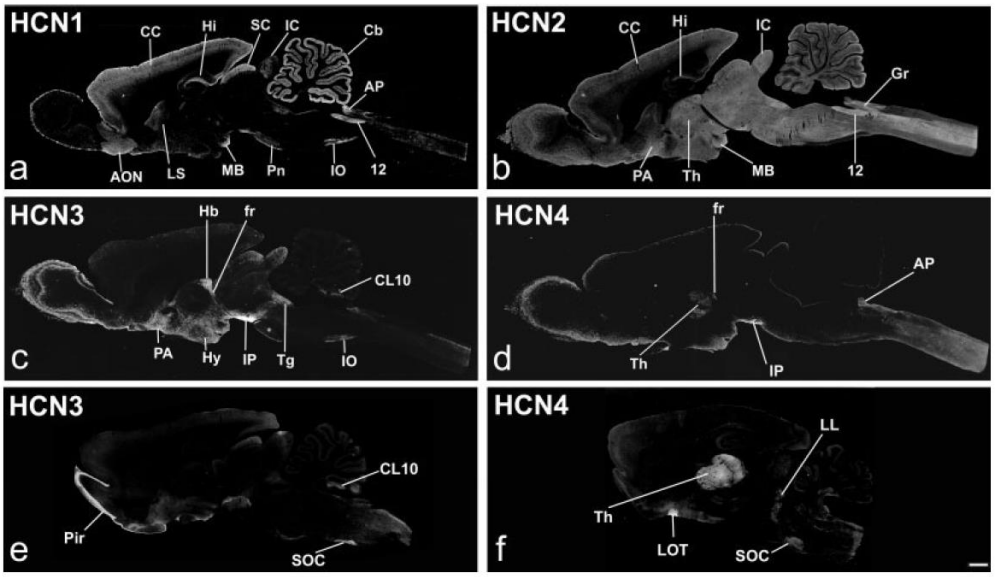

Fig. 3. Distribution of immunoreactivity for HCNs in the rat brain. Parasagittal sections of the rat brain were immunostained with HCN1 (**a**), HCN2 (**b**), HCN3 (**c**,**e**), and HCN4 (**d**,**f**) antibodies. 12, hypoglossal nucleus; AON, anterior olfactory nuclei; AP, area postrema; Cb, cerebellar cortex; CC, cerebral cortex; CL10, cerebellar cortex lobule 10; fr, fasciculus retroflexus; Gr, gracile nucleus; Hb, habenular nucleus; Hy, hypothalamus; Hi, hippocampus; IC, inferior colliculus; IO, inferior olive; IP, interpeduncular nucleus; LOT, nucleus of the lateral olfactory tract; LL, lateral lemniscus; LS, lateral septum nucleus; MB, mammillary body; PA, preoptic area; Pir, piriform cortex; Pn, pontine nuclei; SC, superior colliculus; SOC, superior olivary complex; Tg, tegmental nuclei; Th, thalamus. Scale bar = 1 mm.

Notomi & Shigemoto 2004

THE IUPHAR ION CHANNEL COMPENDIUM

Channel name	HCN4 (refs. 1–4)
Description	hyperpolarisation-activated, cyclic nucleotide-gated cation channel
Other names	HAC4, BCNG3
Molecular information	human: 1203aa, Q9Y3Q4, AJ132429, chr. 15q24-q25, *HCN4* rat: 1198aa, Q9JKA7, AF247453, chromosomal location not established mouse: AF064874, chromosomal location not established
Associated subunits	not established
Functional assays	voltage clamp
Current	I_h or I_f or I_q
Conductance	not established
Ion selectivity	K^+, Na^+ (p_{Na}/p_K ~ 0.2); divalents do not permeate
Activation	$V_{0.5}$ = −65mV to −100mV; τ_a = 260ms–30s at −140mV to −70mV (values are strongly influenced by experimental parameters such as temperature, pH, pulse protocol)
Inactivation	no inactivation
Activators	cAMP > cGMP (both induce a positive shift of $V_{0.5}$ in the range +10mV to +25mV)
Gating inhibitors	ZD7288
Blockers	Cs^+, ZD7288, ivabradine, zatebradine, alinidine
Radioligands	none
Channel distribution	thalamus, retina, olfactory bulb, sinus node, taste cells, testis
Physiological functions	pacemaker activity, resting potential, rebound depolarisations, control of synaptic transmission, transduction of sour taste
Mutations and pathophysiology	homozygous deletion of HCN4 is lethal at embryonic day 10 in mouse
Pharmacological significance	not established
Comments	

REFERENCES

1. Ludwig, A., Zong, X., Stieber, J., Hullin, R., Hofmann, F. and Biel, M. (1999). Two pacemaker channels from human heart with profoundly different activation kinetics. *EMBO J.*, **18**, 2323–2329.
2. Seifert, R., Scholten, A., Gauss, R., Mincheva, A., Lichter, P. and Kaupp, U. B. (1999). Molecular characterization of a slowly gating human hyperpolarization-activated channel predominantly expressed in thalamus, heart, and testis. *Proc. Natl. Acad. Sci. USA*, **96**, 9391–9396.
3. Monteggia, L. M., Eisch, A. J., Tang, M. D., Kaczmarek, L. K. and Nestler, E. J. (2000). Cloning and localization of the hyperpolarization-activated cyclic nucleotide-gated channel family in rat brain. *Brain Res. Mol. Brain Res.*, **81**, 129–139.
4. Ishii, T. M., Takano, M., Xie, L. H., Noma, A. and Ohmori, H. (1999). Molecular characterization of the hyperpolarization-activated cation channel in rabbit heart sinoatrial node. *J. Biol. Chem.*, **274**, 12835–12839.

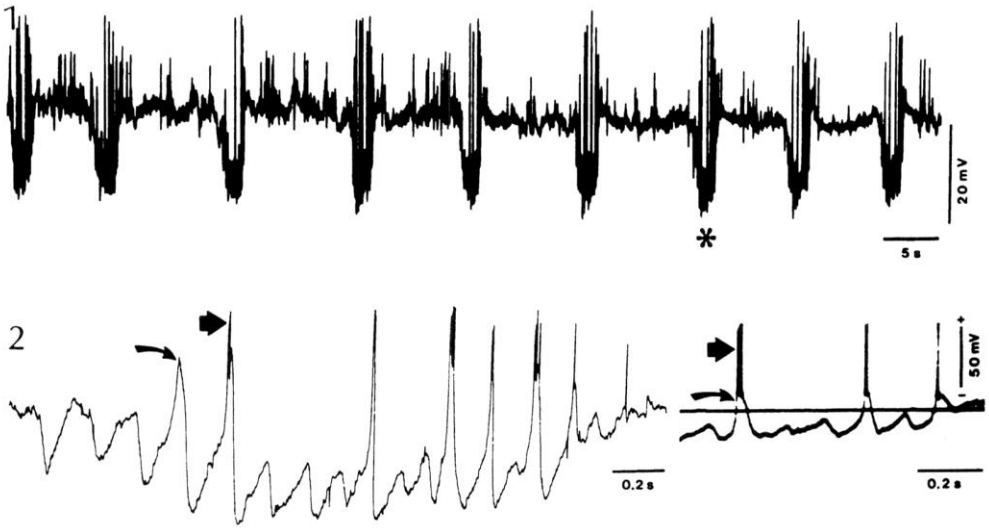

FIG. 4. Spontaneous rhythmic episodes of membrane potential oscillations in a thalamic relay neuron located in the VL nucleus. Spindle sequence marked by an asterisk is depicted below at a faster speed. Traces 1 and 2 are polygraphic recordings. Oscilloscopic recording appears in the right-hand trace in 2. Curved and straight arrows indicate, respectively, the low-threshold Ca spike and somatic burst discharges. In the interspindle lull the membrane potential was −63 mV.

Deschenes et al. 1984

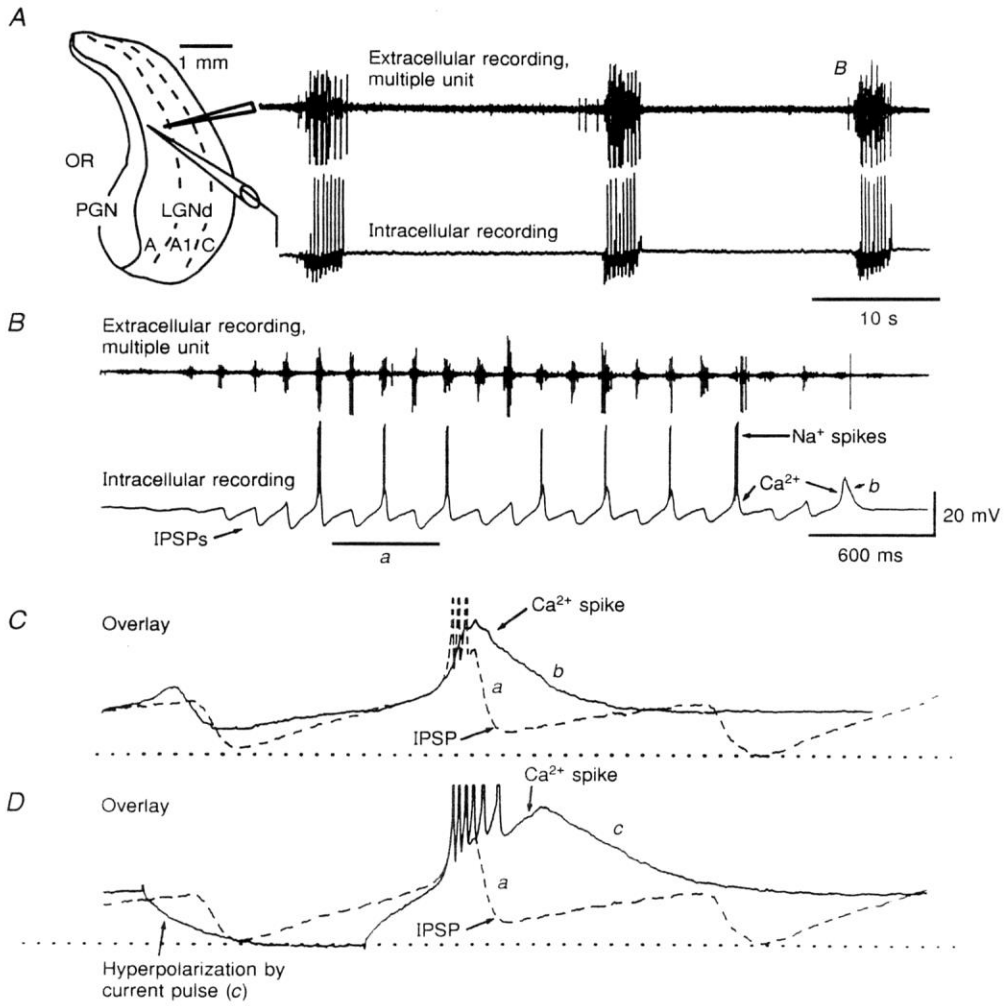

Figure 2. Simultaneous intra- and extracellular recordings in the ferret LGNd slice during spindle wave generation

A, extracellular multiple unit recordings reveal the occurrence of spindle waves (top trace). Intracellular recordings from one relay neuron near the extracellular recording site reveals the arrival of IPSPs during spindle wave generation and the occasional generation of rebound low threshold Ca^{2+} spikes. The drawing depicts a sagittal slice of the ferret LGNd and the locations of the PGN and laminae A, A1 and C, as well as the location of the extracellular and intracellular recording electrodes. The location of the fibres of the optic radiation (OR) are indicated. Anterior is to the left and dorsal is up. *B*, the bursts of action potentials in the intracellularly recorded neuron are in marked synchrony with those recorded with the extracellular electrode. *C*, spindle wave IPSPs appear to overlap substantially with the second half of low threshold Ca^{2+} spikes. Overlaying the IPSP and rebound Ca^{2+} spike (*a*, dashed line) with the last rebound Ca^{2+} spike which was not followed by an IPSP (*b*, continuous line) illustrates how IPSPs shorten the duration of the low threshold Ca^{2+} spikes. *D*, similarly, overlaying an IPSP and rebound Ca^{2+} spike from a spindle wave (*a*, dashed line) and a rebound Ca^{2+} spike after a hyperpolarizing current pulse (*c*, continuous line) illustrates the difference in duration of these rebound Ca^{2+} spikes.

Bal et al. 1995

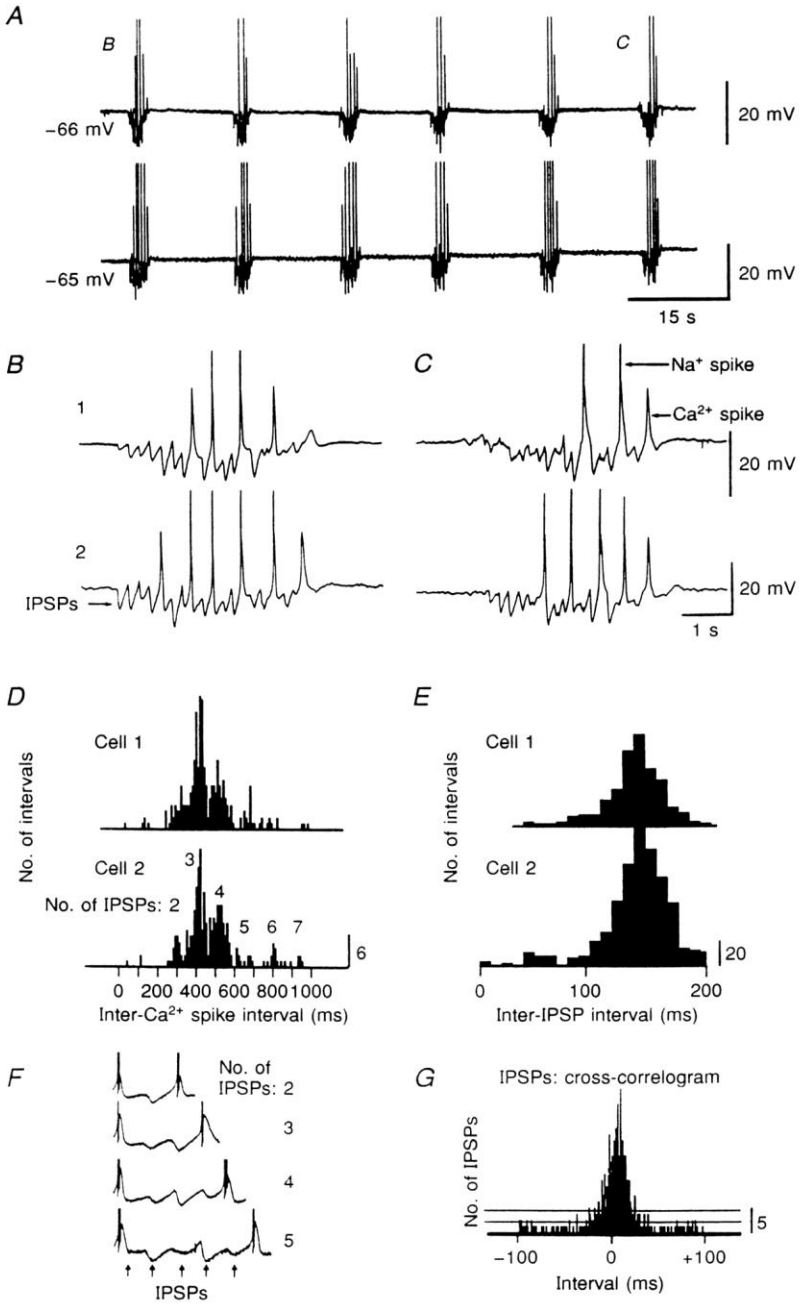

Figure 3. Simultaneous intracellular recordings from two relay cells within close proximity (< 100 μm) of each other

Each relay cell received barrages of IPSPs and generated rebound low threshold Ca^{2+} spikes. The precise timing of rebound Ca^{2+} spike generation varied from cell to cell and spindle wave to spindle wave (*A–C*), as did the amplitude of the individual IPSPs (*B* and *C*). *D*, a plot of the interval between Ca^{2+} spikes during spindle waves for both cells reveals peaks at the times corresponding to the occurrence of 2, 3, 4, 5, 6 and 7 IPSPs, with the largest peak occurring after 3 IPSPs. Examples of rebound Ca^{2+} spikes after 2, 3, 4 and 5 IPSPs are shown in *F*, which is in register with the histogram of *D*. Relay cells typically generate rebound Ca^{2+} spikes at 0·5–4 Hz during spindle wave generation. *E*, interval histogram for the intervals between IPSPs during spindle wave generation for both cells. *G*, cross-correlogram between the IPSPs in cells 1 and 2, showing the marked synchrony between the cells with cell 1 leading cell 2 by approximately 5 ms. Horizontal lines represent one and two standard deviations above average, assuming uncorrelated activity.

Bal et al. 1995

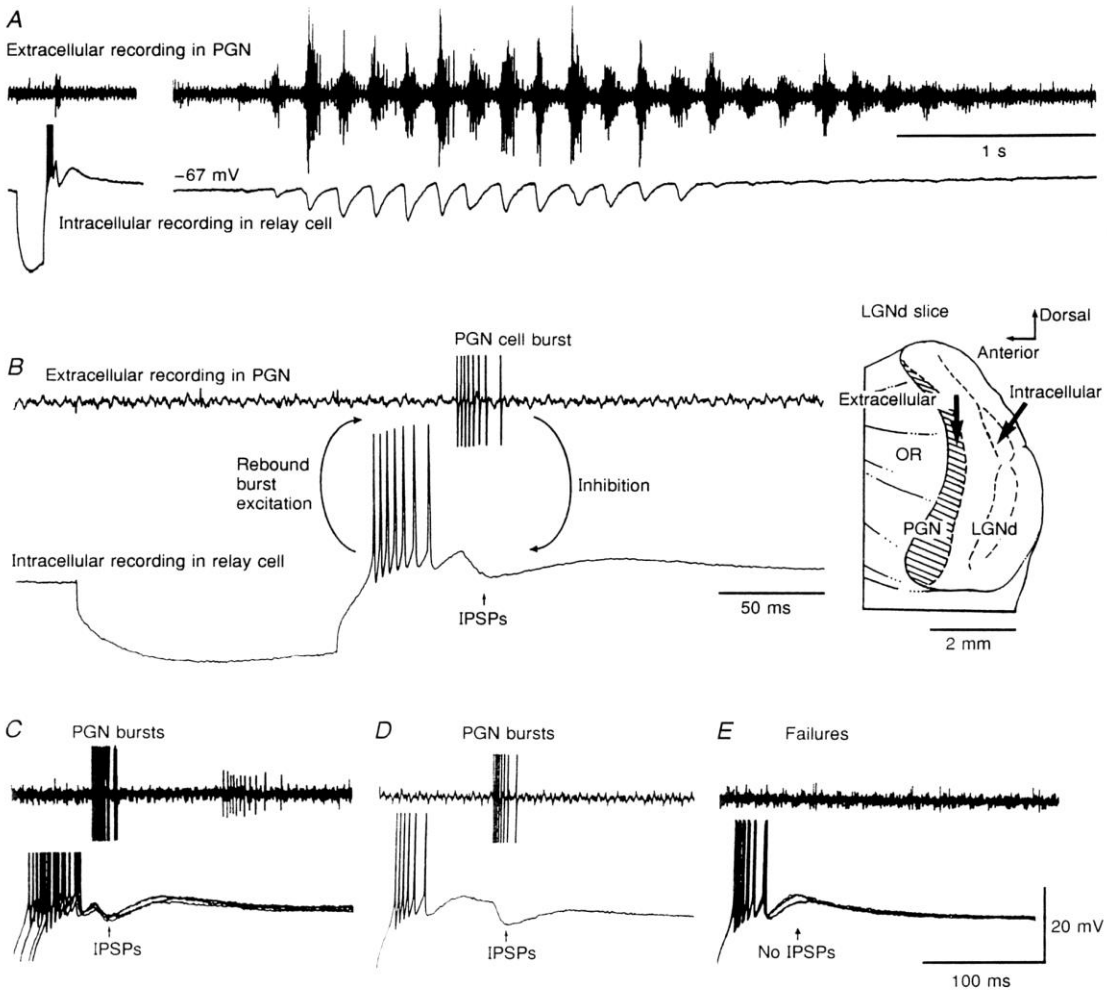

Figure 8. Influence of PGN activity on relay neurons

A, simultaneous intracellular recording from a relay neuron and extracellular multiple and single unit recording from the PGN. Intracellular injection of a hyperpolarizing current pulse in the relay neuron is followed by a rebound burst of action potentials, which is then followed by a burst of action potentials in a PGN neuron. During the generation of a spindle wave, the relay neuron receives barrages of IPSPs in synchrony with bursts of action potentials in the PGN neurons. *B*, expansion of the response of the relay cell to the hyperpolarizing current pulse, the PGN cell bursts, and the subsequent IPSPs in the relay cell. *C*, overlaying 5 simultaneous PGN/LGNd recordings illustrates the time course of the IPSPs. Traces were shifted in time so that the first action potential in the PGN cell matched for each recording. *D*, the onset of the IPSP was delayed when the onset of the burst in the PGN cell was delayed, suggesting that they were related. *E*, when the PGN cell failed to burst, the feedback IPSP also failed, again confirming the reciprocal relationship between the relay and PGN neurons (4 examples are shown).

Bal et al. 1995

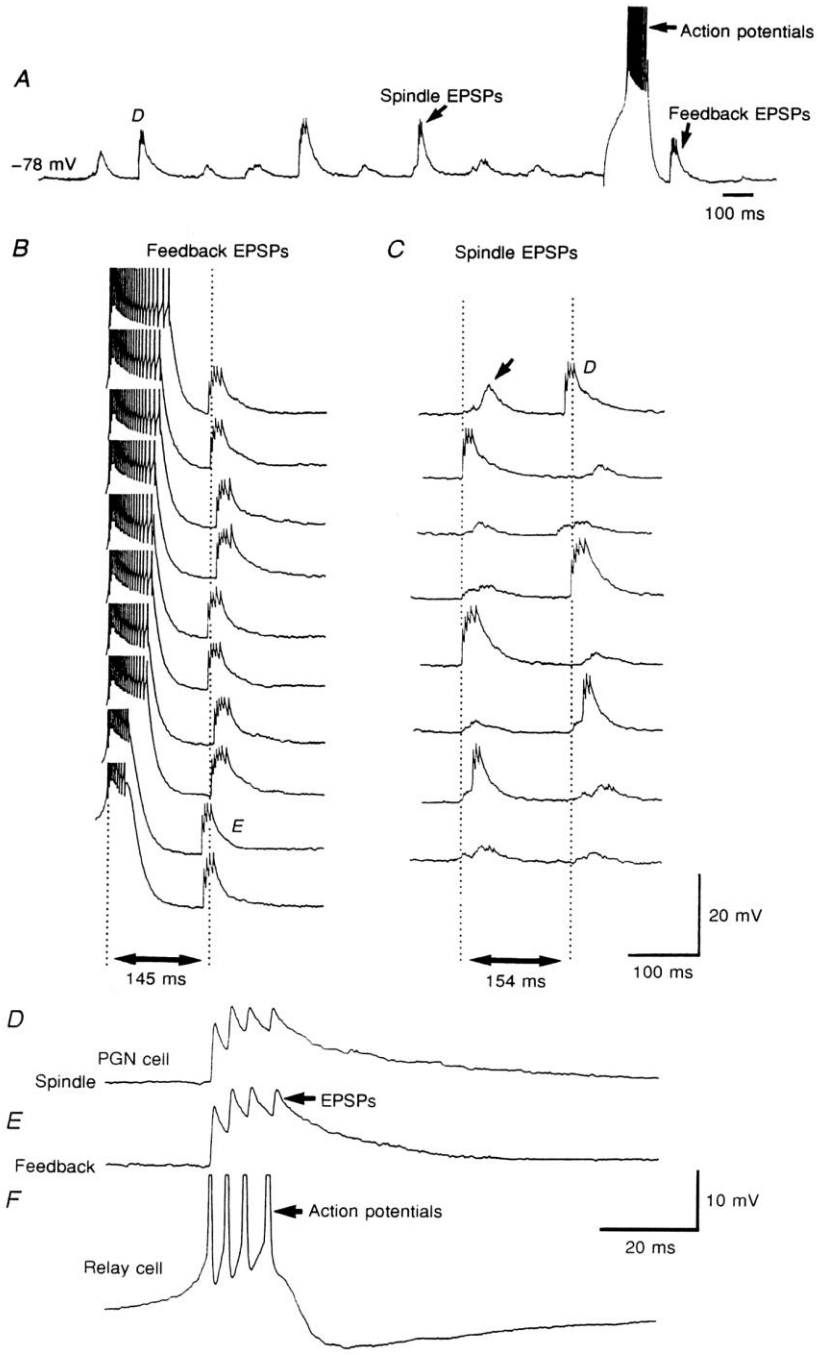

Figure 7. Activation of a PGN neuron results in a burst of feedback EPSPs

A, intracellular recording of a PGN neuron reveals barrages of EPSPs during the generation of a spindle wave. Intracellular injection of a depolarizing current pulse results in a burst of action potentials followed by a barrage of feedback EPSPs (*A*, right). *B*, illustration of feedback EPSPs associated with generation of low threshold Ca^{2+} spikes and bursts of high frequency action potentials in this PGN neuron. The dotted vertical line represents the average latency in this cell of 145 ± 3 ms (S.D.) from the first action potential to the beginning of the barrage of EPSPs. Examination of the interval between barrages of EPSPs in the same neuron during spindle waves revealed an average interval of

Bal et al. 1995

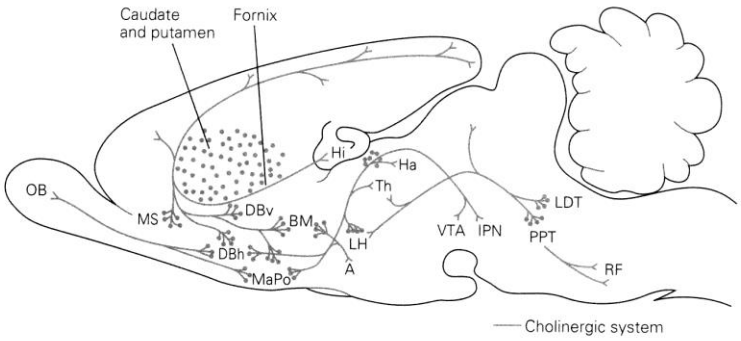

Cholinergic neurons in the upper pontine tegmentum and basal forebrain diffusely innervate much of the brain stem and forebrain. The basal forebrain cholinergic groups include the medial septum (**MS**) (Ch1 group), nuclei of the vertical and horizontal limbs of the diagonal band (**DBv** and **DBh**) (Ch2 and Ch3 groups), and the nucleus basalis of Meynert (**BM**) (Ch4 group), which topographically innervate the entire cerebral cortex, including the hippocampus (**Hi**) and the amygdala (**Am**). The pontine cholinergic neurons, in the laterodorsal (**LDT**) (Ch5 group), and pedunculopontine (**PPT**) (Ch6 group), tegmental nuclei, innervate the brain stem reticular formation (**RF**) as well as the thalamus (**Th**). **Ha** = habenular nucleus; **IPN** = interpeduncular nucleus; **LH** = lateral hypothalamus; **MaPo** = magnocellular preoptic nucleus; **OB** = olfactory bulb; **VTA** = ventral tegmental area.

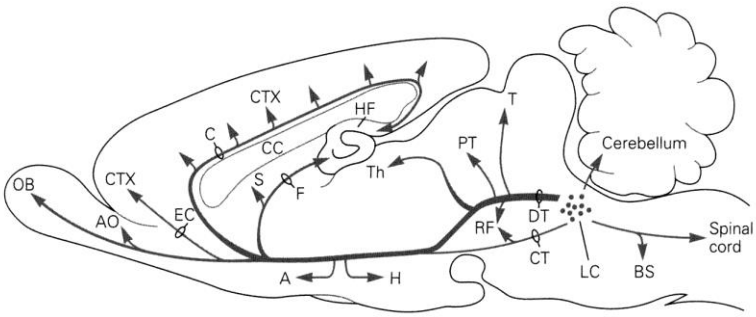

Noradrenergic neurons in the pons.

The A5 and A7 neurons mainly innervate the brain stem and spinal cord, whereas the **locus ceruleus** provides a major ascending output to the thalamus and cerebral cortex as well as descending projections to the brain stem, cerebellum, and spinal cord. **A** = amygdala; **AO** = anterior olfactory nucleus; **BS** = brain stem; **C** = cingulate bundle; **CC** = corpus callosum; **CT** = central tegmental tract; **CTX** = cerebral cortex; **DT** = dorsal tegmental bundle; **EC** = external capsule; **F** = fornix; **H** = hypothalamus; **HF** = hippocampal formation; **LC** = locus ceruleus; **OB** = olfactory bulb; **PT** = pretectal nuclei; **RF** = reticular formation; **S** = septum; **T** = tectum; **Th** = thalamus.

Kandel-Schwartz-Jessel 1991

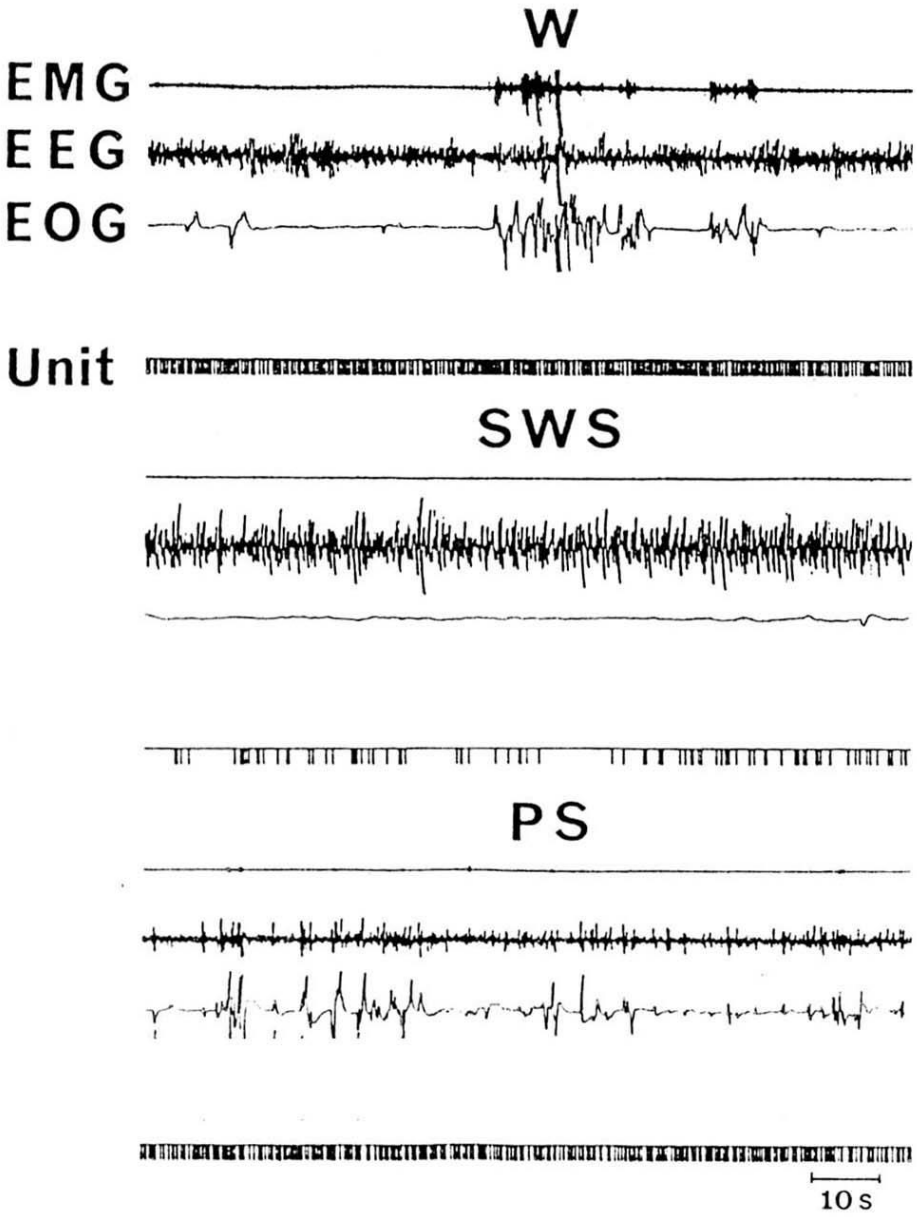

Fig. 5A, Changes in spontaneous unit activity during the sleep-waking cycle of a tonic type I–S neuron (unit)

El Mansari et al. 1989

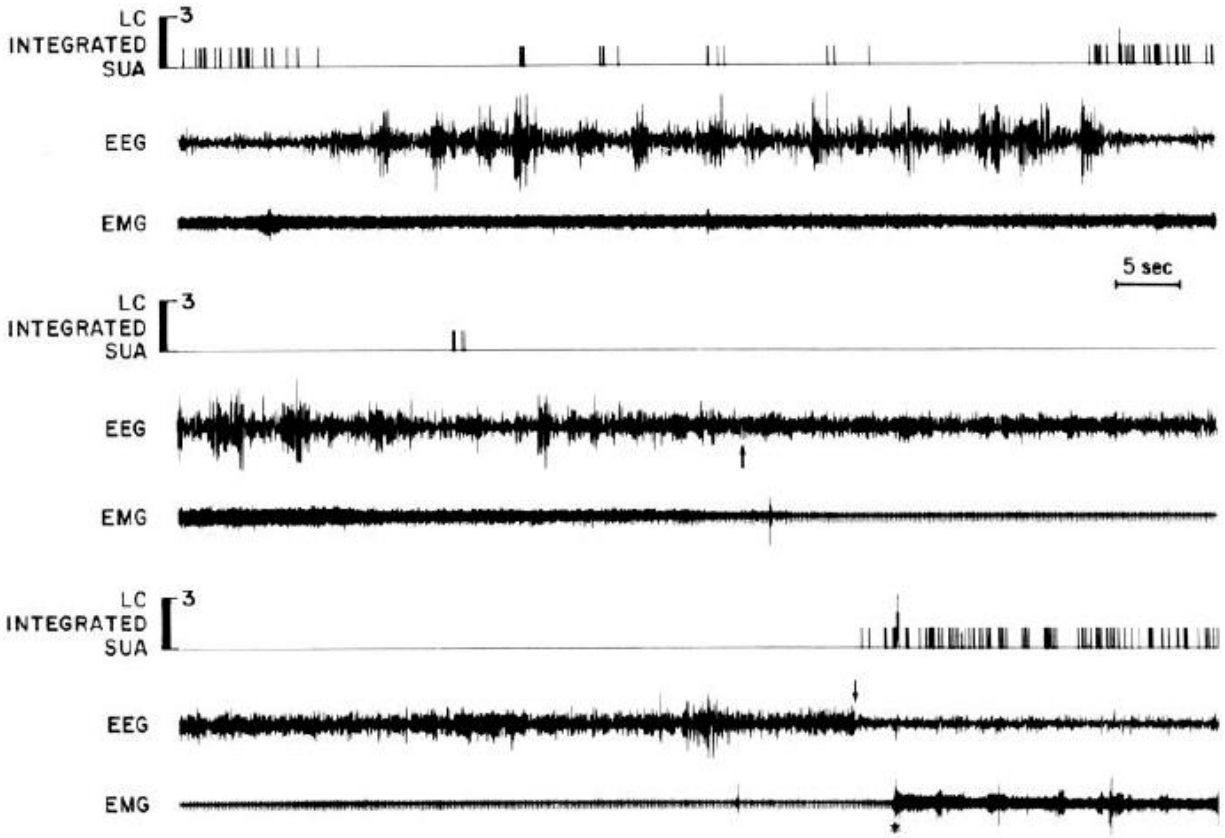

Figure 2. Spontaneous SU activity (*SUA*) during stages of the S-WC. Three epochs from one S-WC for a typical NE-LC single neuron are shown. SWS (high amplitude, low frequency, periodic EEG) contains less discharge than W (low amplitude, aperiodic EEG). Note the altered impulse activity anticipating transitions into and out of SWS and associated with EEG spindles. As is characteristic, discharge is absent during PS (onset at *up arrow*) and returns coincident with EEG-W (*down arrow*) but before EMG-W (*asterisk*). *Top panels* are analog discharge traces taken from epochs (as marked) of one S-WC. *Dots* indicate spikes meeting waveform discriminator criteria. *Upper time calibration bar* refers to *top panels*; *lower bar* refers to all other records.

Aston-Jones & Bloom 1981

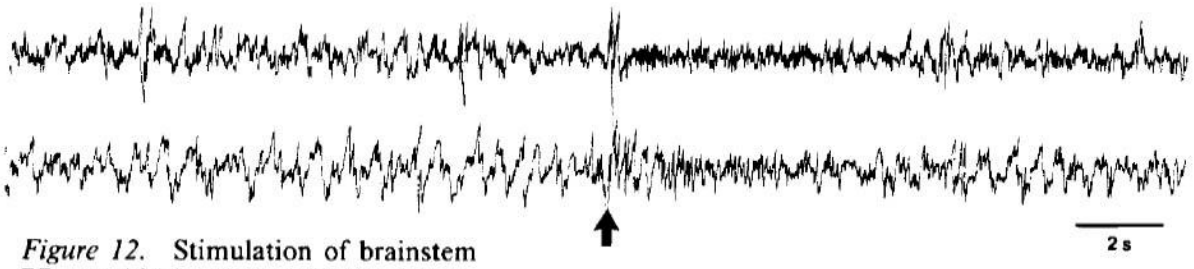

Figure 12. Stimulation of brainstem PB area blocks slow oscillation (extracellular recordings).

Steriade et al. 1991

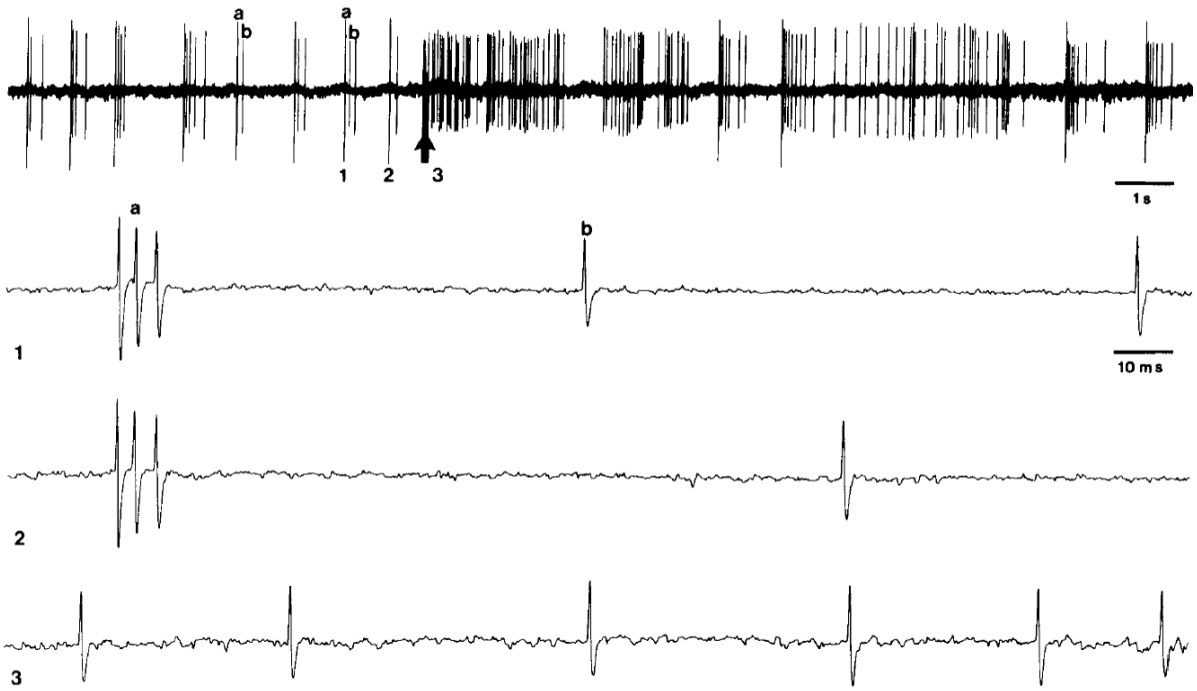

Figure 13. PB-induced blockage of slow oscillation and tonically increased firing in two simultaneously recorded cells in CL nucleus (extracellular recordings). Two cells are labeled *a* (bursting) and *b* (single spikes). PB stimulation (*arrow*) was a 0.1 sec pulse train at 300 Hz. Periods *1–3* indicated on the *top trace* are expanded in the *bottom three traces.*

Steriade et al. 1991

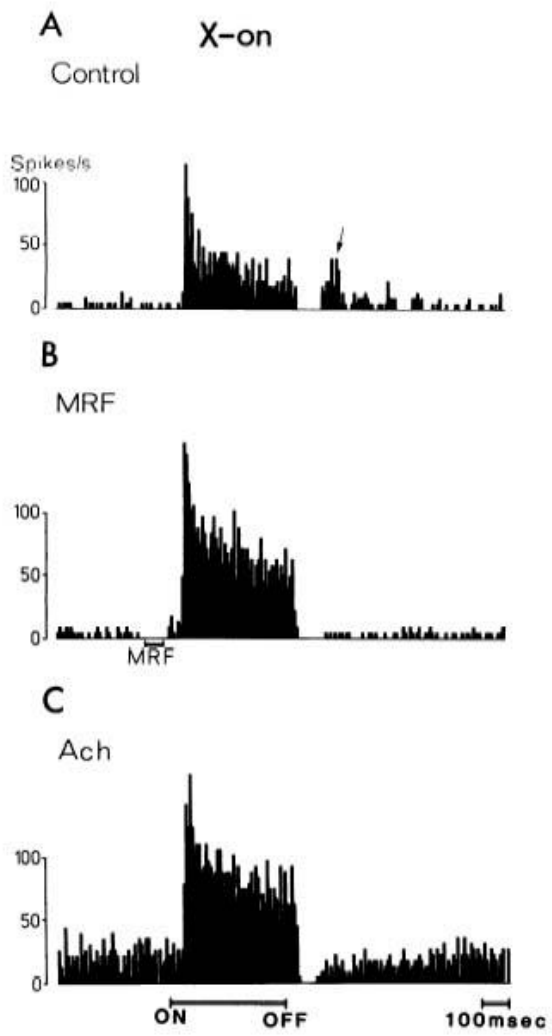

FIG. 2. Peristimulus histograms showing the light responses to a stationary flashed center stimulus in an X-on-center (*A-C*) and a Y-on-center neuron (*D-F*). Histograms *A* and *D* represent responses to the 500-ms-long light stimulus alone. *B* and *E*: mesencephalic reticular formation stimulation was applied 100 ms prior to the onset of the light stimulus and in *C* and *F* acetylcholine was continuously applied with 70 and 20 nA, respectively. *Arrow* in *A* indicates the postinhibitory rebound after light off. *Arrows* in *D* and *F* refer to the delayed on-inhibition. The X-cell was recorded from lamina A1 and responded with 2-ms latency to optic chiasm (OX) stimulation. Recordings were obtained under N_2O/barbiturate anesthesia.

Francesconi et al. 1988

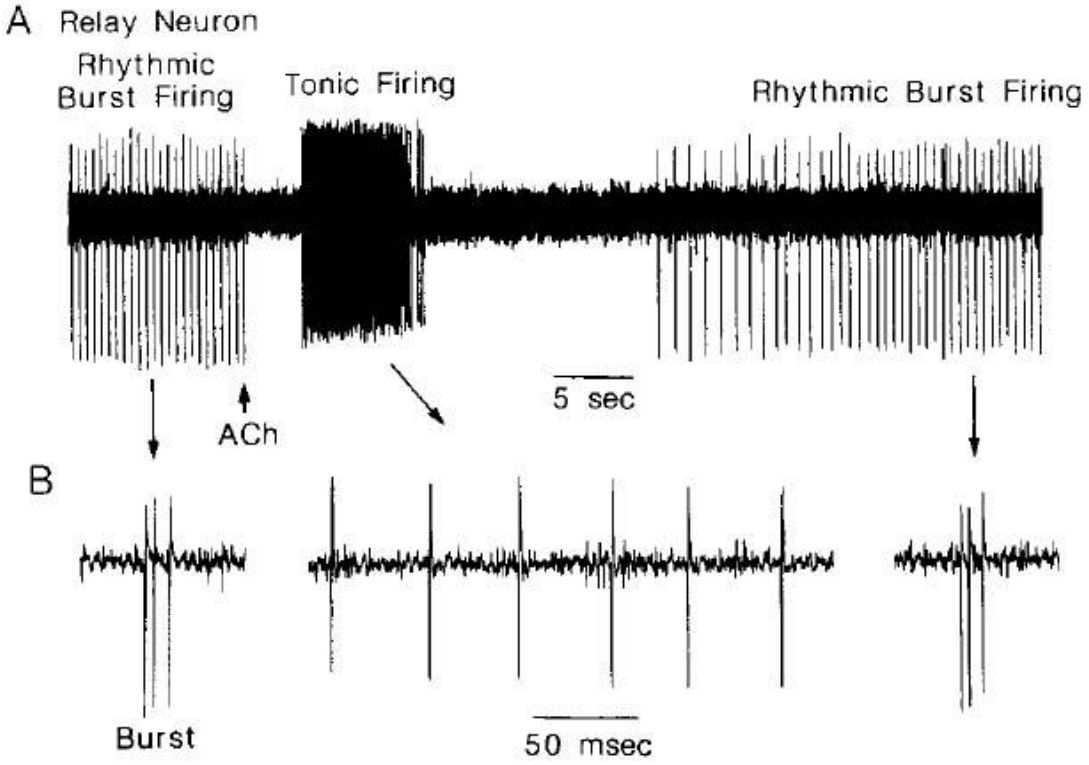

Figure 1. Application of ACh to a rhythmically bursting presumed relay neuron in the cat LGNd results in a cessation of burst activity and the appearance of tonic, or single spike, firing. After a delay, rhythmic burst firing reappears and returns to the baseline frequency of 2 Hz. Each *vertical line* prior to application of ACh represents a high-frequency burst of three to five action potentials. One such burst is expanded for illustration in *B*.

McCormick 1992

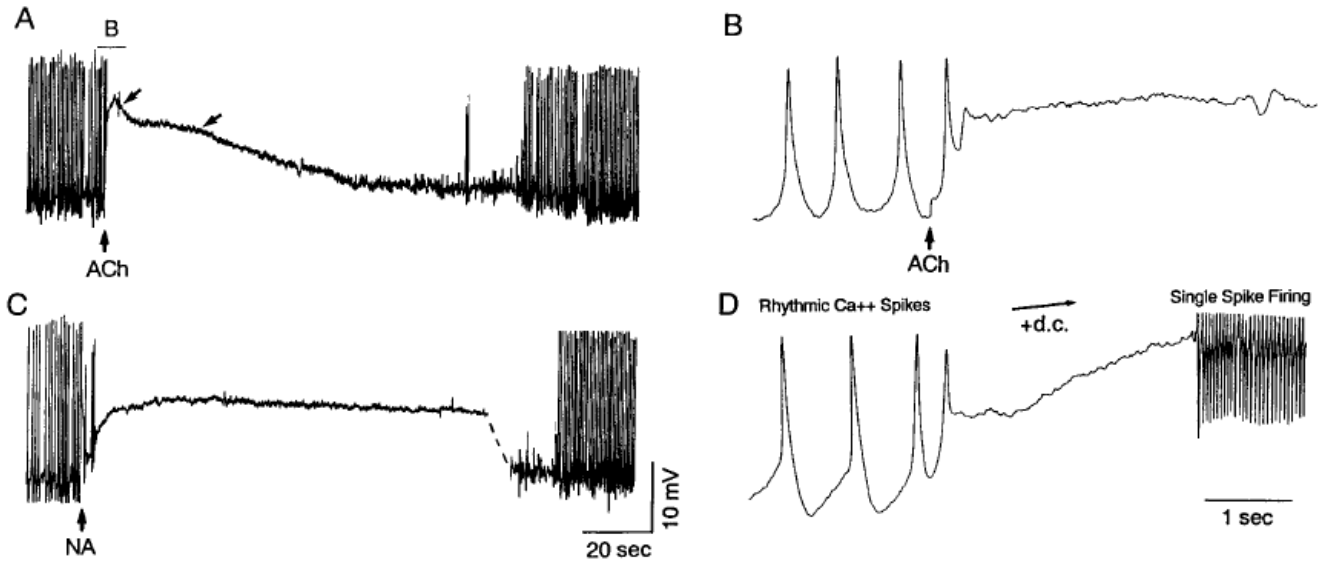

Figure 2. Abolition of the rhythmic generation of Ca^{2+} spikes by ACh and NA in cat LGNd relay neurons. *A,* Intracellular recording of a cat LGNd neuron that spontaneously generated rhythmic Ca^{2+} spikes at resting membrane potential (each *vertical line* is one Ca^{2+} spike) at a rate of approximately 1.5 Hz. In this particular cell, the Ca^{2+} spikes were just subthreshold for the generation of fast Na^+/K^+-mediated action potentials. Application of ACh resulted in a marked depolarization that decayed in two distinct phases (*arrows*). At the end of the response to ACh, rhythmic burst firing reappeared. *B,* Expanded portion of *A* illustrates rhythmic low-threshold Ca^{2+} spikes and depolarization induced by ACh. *C,* Application of NA to this neuron also results in a marked slow depolarization and abolition of rhythmic Ca^{2+} spikes. *D,* Intracellular injection of depolarizing current (+*d.c.*) also resulted in an abolition of rhythmic burst firing and could switch the neuron to the single spike (tonic) mode of action potential generation. All data were obtained from the same cat LGNd neuron in lamina A1. Membrane potential at the most negative point during oscillation was −80 mV.

McCormick 1992

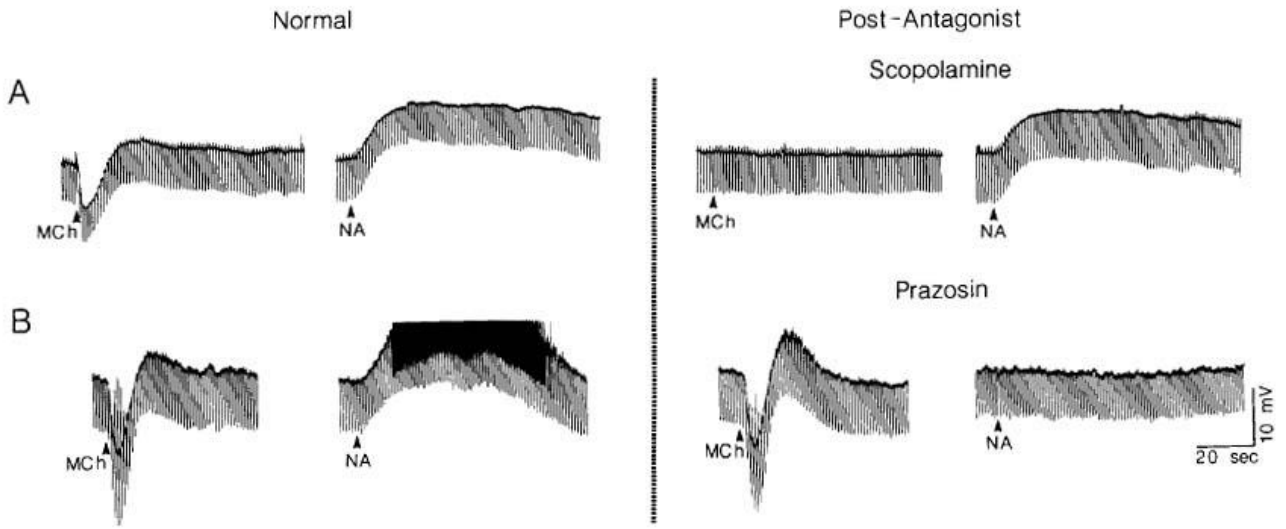

Figure 4. MCh and NA cause slow depolarizations through pharmacologically distinct receptors in guinea pig LGNd. *A,* Local application of scopolamine (10 μM in micropipette) completely blocks the response to MCh, but not to NA. *B,* Local application of the α_1-adrenergic antagonist prazosin (10 μM) completely blocks the slow depolarizing effect of NA, but not of MCh.

McCormick 1992

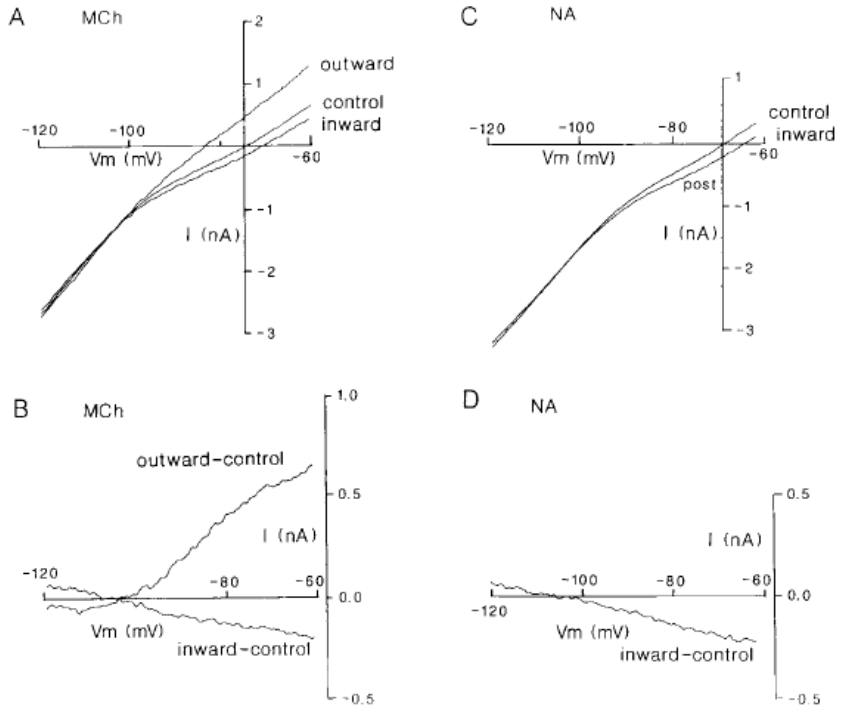

Figure 5. Voltage dependence of responses to MCh and NA. *A*, Current versus voltage plots obtained before (*control*), during the outward current (*outward*), and during the inward current (*inward*) responses activated in response to local application of MCh. *B*, Subtraction of control *I–V* plots from those obtained during the outward or inward currents reveal the voltage dependence of these two responses. *C*, *I–V* relations before (*control*) and during the NA-induced inward current (*inward*). *D*, Subtraction of control *I–V* plots from the inward current plots reveal that the affected current varies in a relatively linear manner with membrane potential. All data obtained from the same guinea pig LGNd cell in normal bathing medium.

McCormick 1992

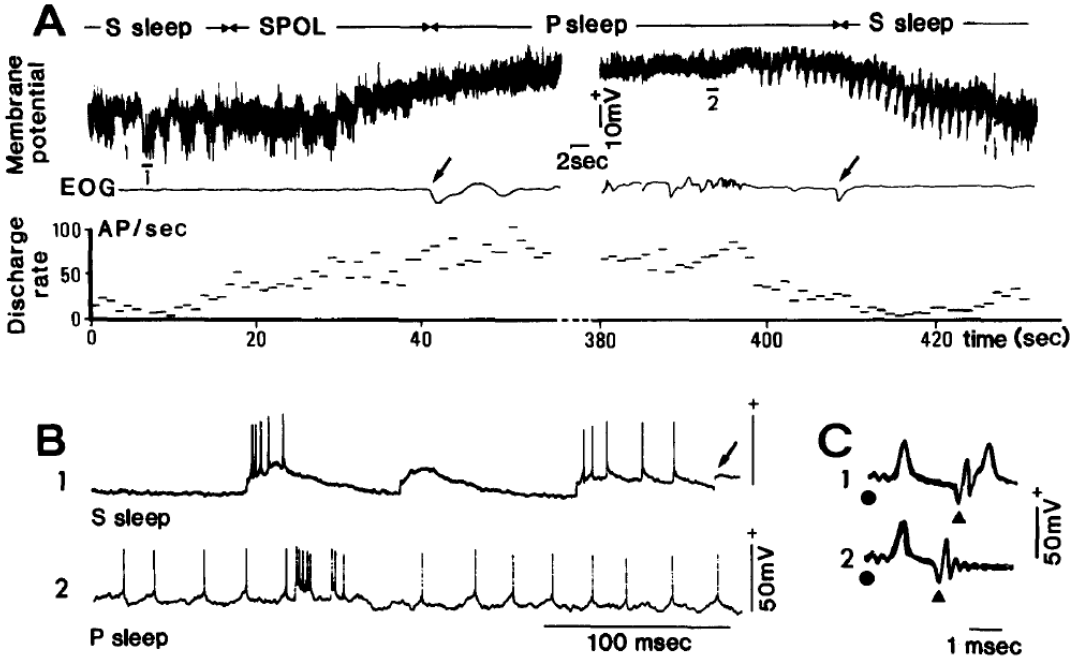

Fig. 1. Tonic depolarization of an LGB realy neuron during P sleep. A: simultaneous display of behavioral state. DC cell recording (filtered at 0–75 Hz), eye movements (EOG) and discharge rate of action potentials (bin width: 1 s). Left-hand side: neuron depolarized during SPOL and had already depolarized by 8 mV when the animal entered P sleep (t = 41 s, first eye movement, arrow). Depolarization was maintained throughout P sleep; only the beginning and the end of the episode is presented (320 s elapsed between left and right sets of traces). Right-hand side: upon last eye movement (arrow) of P sleep the neuron repolarized as the animal went back to S sleep. B: enlarged segments (labelled 1 and 2 under cell trace in A) of spontaneous activity. B_1: S sleep activity was composed of isolated EPSPs (arrow) that did not always fire the cell and of large depolarizations with or without a burst of spikes. B_2: during P sleep action potentials arose from small depolarizations. The rapid discharge was disrupted by short depolarizations which gave birth to a cluster of spikes of decreasing amplitude. C: identification of neuron. C_1: orthodromic response to optic tract stimulation (circle), antidromic action potentials to visual radiation stimulation (triangle). C_2: positive collision test. Five traces superimposed.

Hirsch et al. 1983

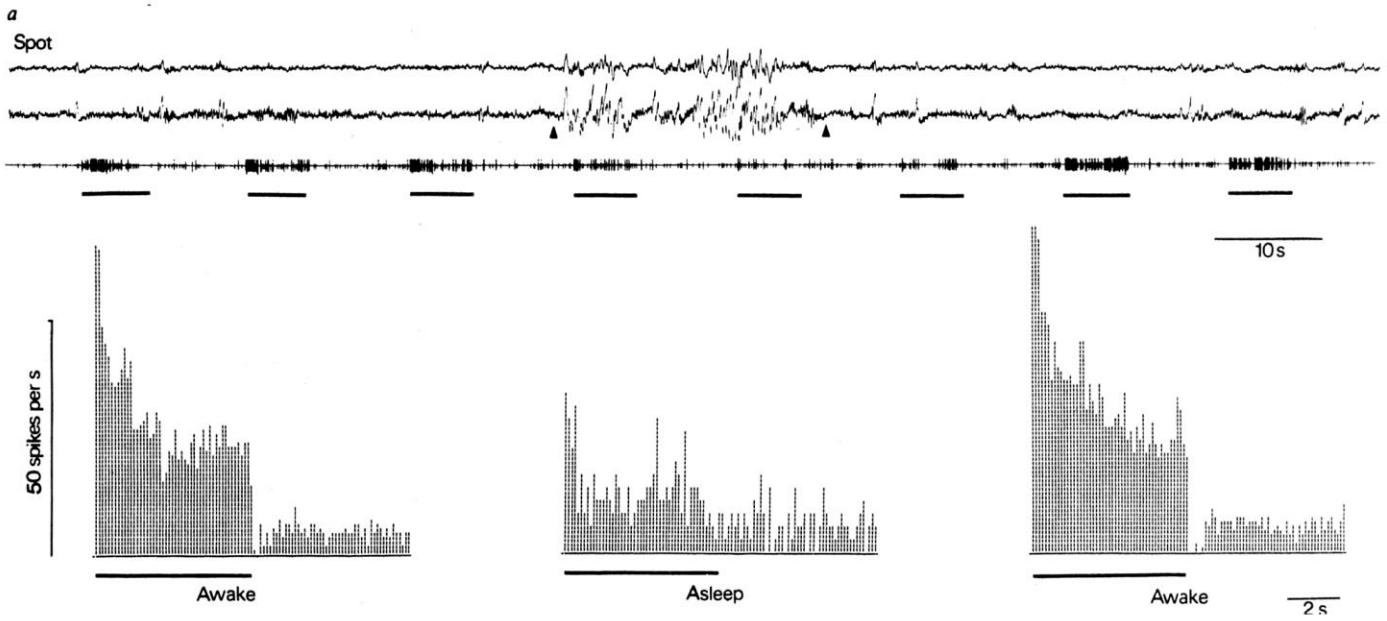

Fig. 1 *a* and *b*, Responses of an on-centre cell from layer A of the lateral geniculate nucleus in a drowsy cat. In each polygraph record the upper two traces are the bipolar EEGs from anterior and posterior head regions; the third trace shows the spikes from the geniculate cell, converted into pulses, in these and subsequent polygraph records, by a Schmitt trigger circuit. Each record lasts ~2 min. Brief periods of sleep, which end spontaneously, are indicated by the slow waves in the middle of record *a* and (roughly) the left half of *b*. The approximate transitions between the flat waking EEG record and periods of slow-wave sleep are indicated by arrowheads. In *a* a spot covering the receptive field centre is flashed on and off. The relative weakness of the on responses during periods of slow waves can be seen in the record of spikes and in the three histograms. The left histogram is the average of 13 responses, of which the last 3 are shown. The middle histogram is an average of the 2 responses during the burst of slow waves, and the right histogram the average of the next 16 responses.

Livingsone & Hubel 1981